Signal Processing Systems
Mekelweg 4,
2628 CD Delft
The Netherlands
https://sps.ewi.tudelft.nl/

SPS-2023-5534615

M.Sc. Thesis

Interpretable Parametric Modelling of the Heart based on ECG Signals

Chengyan Wang

Abstract

Atrial fibrillation (AF) is one of the most common heart diseases. Billions of people have suffered from it in the world. Although it can lead to terrible complications such as stroke and heart failure, the underlying mechanisms of it are still under-explored. Besides, there is no so-called optimal therapy for the patients. As the disease is progressive, it is important to detect it in an early stage. To develop methods for understanding and detecting AF, the interpretable parametric model can be an option. This model can provide physiological information at the signal level. In this case, the electrocardiogram, as the most commonly used invasive measurement of cardiac conditions, can be the data to model the heart structure and cardiac activities.

This thesis proposes an interpretable parametric model based on P-waves extracted from the ECG signals. Specifically, the autoregressive (AR) model is implemented, which is also known as linear predicting coding (LPC). The goal is to model the atrium and understand the function of the atrium, which can reflect on the varying parameters in the SR and AF cases. In this context, The formant of P-waves is modeled and estimated, which is a representation of the atrium activities. In addition, the parameters of the model are mapped into 2-dimension by the zero-pole plots in order to interpret the differences between SR and AF situations. Based on the differences between parameters and formants, a parametric classifier of high interpretability is developed to detect AF. An alternating searching algorithm is proposed to determine the parameters of the classifier.

Interpretable Parametric Modelling of the Heart based on ECG Signals

Thesis

submitted in partial fulfillment of the
requirements for the degree of

Master of Science

in

Electrical Engineering

by

Chengyan Wang
born in Chongqing, China

This work was performed in:

Signal Processing Systems Group
Department of Microelectronics
Faculty of Electrical Engineering, Mathematics and Computer Science
Delft University of Technology

Delft University of Technology

Delft University of Technology
Department of
Microelectronics

The undersigned hereby certify that they have read and recommend to the Faculty of Electrical Engineering, Mathematics and Computer Science for acceptance a thesis entitled **"Interpretable Parametric Modelling of the Heart based on ECG Signals"** by **Chengyan Wang** in partial fulfillment of the requirements for the degree of **Master of Science**.

Dated: My Graduation Date

Chairman:

Dr.ir. R.C. Hendriks

Advisors:

Dr.ir. R.C. Hendriks

Dr. C. Varon

Committee Members:

Dr.ir. R.C. Hendriks Committee-Member

Dr. C. Varon Member

Dr. C.M.F. Viellard-Boutry Member

Abstract

Atrial fibrillation (AF) is one of the most common heart diseases. Billions of people have suffered from it in the world. Although it can lead to terrible complications such as stroke and heart failure, the underlying mechanisms of it are still under-explored. Besides, there is no so-called optimal therapy for the patients. As the disease is progressive, it is important to detect it in an early stage. To develop methods for understanding and detecting AF, the interpretable parametric model can be an option. This model can provide physiological information at the signal level. In this case, the electrocardiogram, as the most commonly used invasive measurement of cardiac conditions, can be the data to model the heart structure and cardiac activities.

This thesis proposes an interpretable parametric model based on P-waves extracted from the ECG signals. Specifically, the autoregressive (AR) model is implemented, which is also known as linear predicting coding (LPC). The goal is to model the atrium and understand the function of the atrium, which can reflect on the varying parameters in the SR and AF cases. In this context, The formant of P-waves is modeled and estimated, which is a representation of the atrium activities. In addition, the parameters of the model are mapped into 2-dimension by the zero-pole plots in order to interpret the differences between SR and AF situations. Based on the differences between parameters and formants, a parametric classifier of high interpretability is developed to detect AF. An alternating searching algorithm is proposed to determine the parameters of the classifier.

Acknowledgments

Finally, I arrive here with excitement, as the end of my master journey in TU Delft. Looking back at the past two years, I have met many friends and professors, overcome many difficulties with their accompanies, and harvested lots of joyful fruits. I want to express my heartful gratitude to those people who have supported and motivated me to continue my way.

I would like to first thank my advisors Dr.ir. R.C. Hendriksand Dr. C. Varon for their assistance throughout the whole thesis journey. Without them, I could not find out which direction was the right one when I encountered problems. Also, their critical asking and valuable suggestions contributed to the formation of this thesis report. Even more, not only do they support me in an academic way, but also give me tolerance and comfort when I suffer from my disease.

Next, I want to thank my close friends and roommates on the 18th floor of the EWI building: Bingxiang, Haobo, Kunlei, and Xuan. I could not forget the time we discussed research questions, talked about life affairs, and enjoyed the view of day and night in Delft. Your accompanies are the most precious thing I would like to cherish forever. Besides, I want to thank my parents for their support, understanding, and encouragement of my every choice. Thank you for always standing by my side.

Chengyan Wang
Delft, The Netherlands
4th, September, 2023

Acronyms

ADF Augmented Dickey-Fuller. 24

AF Atrial Fibrillation. 1

AIC Akaike information criterion. 30

AR Autoregressive. 1, 2

ARMA Autoregressive moving average. 12

AUC Area under curve. 62

AV Atrioventricular. 5

AWL Average window length. 22

BIC Bayesian information criterion. 30

ECG Electrocardiogram. 1

EGM Electrogram. 7

f-waves Fibrillatory waves. 8

LPC Linear prediction Coding. 11

MLE Maximum likelihood estimation. 27

MSE Minimum squared error. 11

MWL Minimum window length. 22

ODE Ordinary differential equations. 34

PACF Partial autocorrelation function. 29

PSD Power spectral density. 9

ROC Receiver operating characteristic. 62

RSA Respiratory sinus arrhythmia. 8

SA Sinoatrial. 5

SR Sinus Rhythm. 6

Contents

List of Figures

List of Tables

1 Introduction

Atrial Fibrillation (AF) is an abnormal heart rhythm (arrhythmia) but common in people, especially people of old age [1]. It is characterized by rapid and irregular beating of the heart's atrial chambers, which is dangerous since it can increase the risk of stroke, heart failure, and other cardiovascular diseases. It remains a critical cause of disability and death for elderly people [2]. According to statistical data, the prevalence of AF varies from 0.12%–0.16% of people younger than 49 years to 10%–17% of those aged 80 years or older [3].

Although AF is a serious problem threatening individuals' lives, its origin is not yet completely understood. Various mechanisms contribute to the initiation of AF. In general, these mechanisms are represented by ectopic atrial firing and atrial substrates that are generated by dysfunctional cells that promote AF [4]. In this case, it can be concluded that AF occurs due to atrial dysfunction, and many researchers pay efforts to investigate AF from a cellular level. One way to do so is using invasive measurements. However, non-invasive measuring measurements are preferred from a patient's point of view and the cost perspective.

The Electrocardiogram (ECG) is the most well-known noninvasive method to collect cardiac measurements from patients. With an ECG, cardiac activities are mapped to the recordings. Accordingly, the information cardiac activities provide can be obtained and atrial dysfunction can be analyzed at the signal level [5]. Signal-processing models can be used to deal with the waves representing cardiac activities. To guarantee a certain degree of interpretability of the information obtained, the signal-processing techniques should be parametric as opposed to non-parametric blind methods like machine learning techniques.

1.1 The Main Problem

Although AF influences a large number of people, the underlying mechanism is a controversial topic, which is not revealed completely. Besides, nowadays, many researchers favor exploiting machine learning and deep learning to deal with ECG signals and overlook the interpretation of AF initiations. Hence, to tackle the interpretable information behind the AF and atrium, a parametric signal model is investigated, whose parameters can represent atrial activities. If the SR and AF differences characterized by model parameters are investigated, it is beneficial to analyze AF mechanisms. Among those parametric models, the autoregressive model (AR) is used to characterize the vocal tract in order to describe the function of voicing. Motivated by this idea, it may be also possible to model the atrium in a similar logic. Hence, in this thesis, the parametric

Autoregressive (AR) model is implemented to obtain the information related to atrial activities such that differences between the SR and AF can be studied. Furthermore, with such differences, classification can be made to detect AF occurrence. Combining the atrium model and the classification model, the overall model can be a black box offering results and information and easy to use for patients and doctors.

1.2 Research Objectives

As discussed above, the objective of this thesis is to construct an interpretable parametric model to explore the pathology of AF at the signal level.

The whole model can be divided into the below questions plus one task:

1. How to model the atrium parametrically based on P-waves?
2. How to interpret information from the parameters of proposed models?
3. How to classify the SR and AF signals in an interpretable manner based on the information obtained from the atrium model?
4. How to determine the parameters of the proposed classifier optimally?
5. Task: To model the atrium, P-waves should be extracted from the ECG recordings, which needs to be done before the Question 1, 2, 3, and 4.

1.3 Outline

The thesis is organized by following the logic of the framework in Fig. 1.1: the relevant background information, which includes the morphology of an ECG signal and modeling techniques, will be given in Chapter 2. Chapter 3 will provide the work about obtaining and then modeling the P-waves, including the preprocessing step and the atrium modeling in Fig. 1.1. The results after pre-processing and modeling, accompanied by some discussion, will also be shown in this chapter. Chapter 4 will mainly focus on interpreting the information obtained from the atrium model and parameters related to zero-pole computation and formant estimation, i.e., interpretation block in Fig. 1.1. The atrium information provided by the model will also be obtained in this chapter. Results and discussion related to the interpretation will be given in this chapter. In Chapter 5, the classification based on parameters and information provided by the model will be proposed. An alternating parameter identification algorithm will also be proposed to determine the parameters of the classifier numerically. In addition, the results of the determination and the classification will be discussed in this part. Finally, chapter 6 will conclude the thesis, list the model's limitations, and present recommendations for future work.

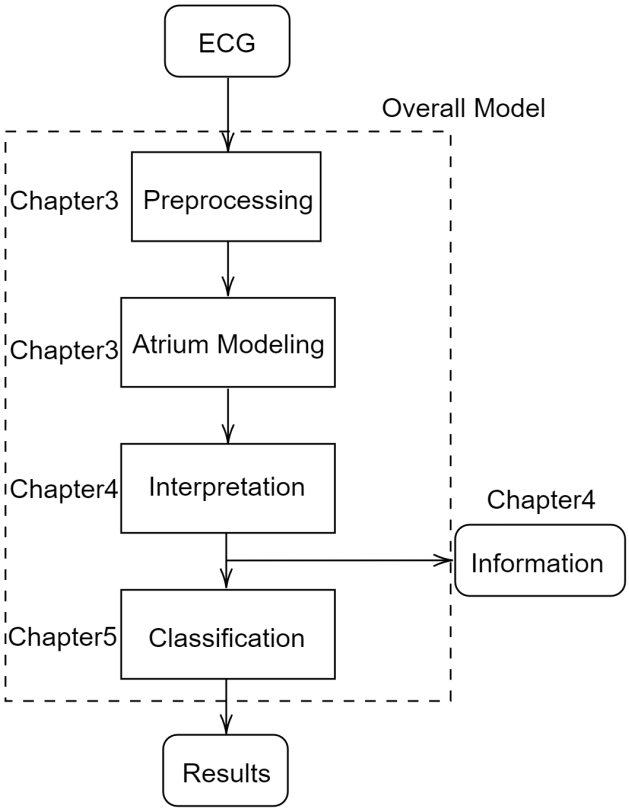

Figure 1.1: The framework of the model designed.

2 Background

This chapter aims to provide some background information related to the thesis. Preliminary knowledge and models will be included. Firstly, the heart in normal condition will be introduced in Section 2.1. Secondly, atrial fibrillation and some known mechanisms will be discussed in Section. 2.2. Next, the commonly-used cardiac measurements will be discussed in Section. 2.3. Some background knowledge related to the ECG will also be provided in that section. Then, models used in the thesis to model the atrium will be introduced in Section. 2.4. They are the autoregressive model and the autoregressive moving average model. In addition, the formant modeling of the AR model will be introduced, which allows it to represent the atrium at the signal level. Last, Section. 2.5 will give the problem formulation of this thesis.

2.1 Heart in Sinus Rhythm

The human heart consists of four chambers: the right atrium, the left atrium, the right ventricle, and the left ventricle. Besides these chambers, there are muscles called myocardium stimulating the heart to contract and drive blood circulation in the body [6]. The chambers and pacemakers are shown in Fig .2.1. The SA node at the right atrium's upper back wall is the starting point of the contraction [7]. It generates electricity rhythmically. These electric impulses come across the atrium and arrive at the atrioventricular (AV) node. During this process, the contraction of the cardiac muscles is stimulated by the propagation of the current. Passing the AV node, the electricity then enters the ventricle. Similar stimulations happen in the ventricle, and the muscles contract.

The contraction of the myocardium represents action potential at the cellular level [8]. It is caused by the change in membrane potential levels. There are three phases in the action potential: depolarization, repolarization, and hyperpolarization [9]. A real record of the action potential is shown in Fig. 2.2. When the membrane potential reaches the threshold, a rapid change in membrane potential occurs as an action potential. The membrane potential increases due to the influx of the positively charged sodium ions (Na+) in the rising phase known as 'depolarization'. The falling phase is called 'repolarization'. The slow decrease of the voltage after the repolarization is 'hyperpolarization'.

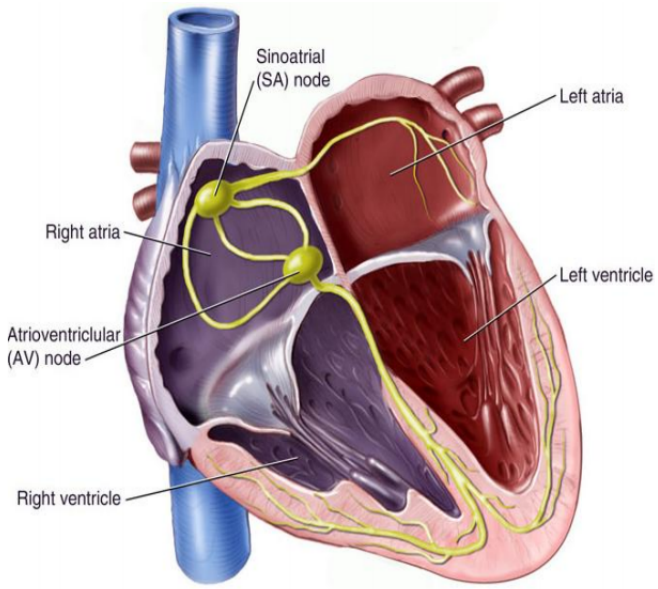

Figure 2.1: Natural pacemakers in the heart. Source: [6]

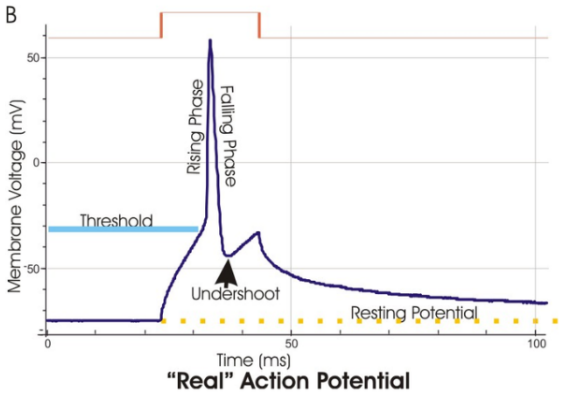

Figure 2.2: A real action potential record. Source: [9]

For the heart in the normal situation, the SA node sends the pulses continuously and rhythmically, and the electricity propagates smoothly. In this case, the depolarization and repolarization of cardiac muscles happen rhythmically. This kind of rhythm is called sinus rhythm (SR).

2.2 Atrial Fibrillation

Atrial fibrillation is an abnormal heart rhythm arising in the heart, resulting in irregular beating due to the pathological change in the atrium. It can be categorized as paroxysmal AF (lasting less than seven days) and persistent AF (lasting more than seven days or requiring cardioversion at any time) in terms of the duration and the recurrent nature of arrhythmic episodes [10]. However, the condition of AF is dynamic:

paroxysmal AF may be developed into persistent if not much attention and health care are being paid. AF induces the electricity alternation in the myocardium, and this electricity abnormality will promote the process by triggering myocardial apoptosis and fibrosis [11]. In this case, 'AF begets AF'.

Lots of research has been done to explore reasons for initiating AF, whereas the underlying mechanism of AF are not fully understood. Many researchers hold the idea that AF is based on different various intimating mechanisms [4]. Some related explanations are focal ectopic firing, which starts from the myocyte sleeves located in the pulmonary veins, and the myocardial apoptosis and fibrosis [12–14]. And the previous consensus of AF that it results from the interplay between the changes in the myocardium and the structural remodeling induced by AF itself has been challenged by observations of the progressive structural abnormalities occurring independently of the cardiovascular comorbidities and persistence of AF [15]. Accordingly, the mechanisms beneath AF are still under-explored.

Although the underlying cause of AF is not yet revealed, what is clear is that this atrial irregular activity results in abnormal electrogram (EGM) or ECG, which are cardiac measurements.

2.3 Measurements of Heart Activity

People have developed different categories of measurements to get information from the heart. The two most commonly used ones are the EGM and the ECG, which will be introduced in this section.

2.3.1 EGM

Myocardial cells generate the cardiac action potentials rhythmically. Although a unipolar system is sometimes used to detect these potentials, a bipolar one is preferred in most cases. The bipolar electrode placed on the heart is a combination of two poles recording potentials generated by various cells in its field of measurement. Usually, these sensors are intracardiac and placed on the atrium. In this case, the EGM only contains the atrial information and does not includes many muscle and tissue noises [5]. However, it also means an EGM is invasive and not applicable to most people.

2.3.2 ECG

As mentioned in Section. 2.3.1, the EGM is invasive and thus is not convenient for patients. A non-invasive method is more practical to implement and more acceptable for patients, favoring the ECG. The surface ECG is the most common measurement for detecting cardiac arrhythmia, especially AF, in the clinical case. The signal is sensed by a number of electrodes put on different locations on the body. The standard 12-lead system, where ten electrodes placed on the body collect data from 12 different locations, is the most preferable and can provide the most accurate information among

all types of ECG signals [16]. Though sacrificing the accuracy and capacity of collecting information, fewer lead systems are more convenient for patients to wear. Meanwhile, systems with fewer leads, like the single-lead system, can also offer sufficient information about AF [17].

An example of a SR ECG signal in one period is shown in Fig. 2.3. On the ECG, the P wave representing the atrial depolarization is the first wave right before the QRS wave. Next to the P wave, the QRS wave with the highest amplitude takes the most prominent position in an ECG period. It indicates ventricular depolarization. After the QRS wave, the T wave appears indicating the ventricular repolarization. For a SR signal, an interval between two successive R peaks called a RR interval is regular since the rhythmical electricity passes the heart without any interference.

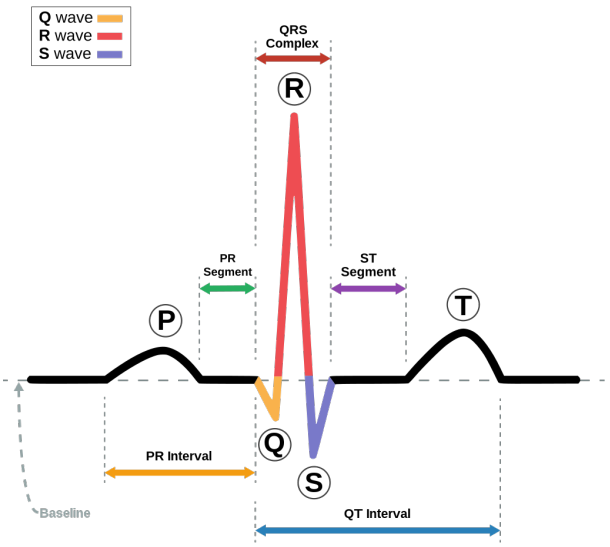

Figure 2.3: Waveform of a standard ECG signal. Source: [18].

As for the AF signal, there are three characteristics:

- irregular RR intervals,
- the presence of fibrillatory waves (f-waves) due to the undulating atrial activity, and
- the absence of repeating P waves.

An example of the ECG signal in AF is shown in Fig. 2.4, where the blue dots mark the R peaks for better elaboration. It can be observed that f-waves replace the P waves. In addition, the RR intervals become irregular, because the electricity conduction gets disturbed. However, one thing to be noted is that a healthy heart can also perform slight RR irregularity due to respiratory sinus arrhythmia (RSA), a natural heart rate

variability in synchrony with respiration [19]. It manifests itself as a shorter R-R interval during inspiration and a longer RR interval during expiration [20].

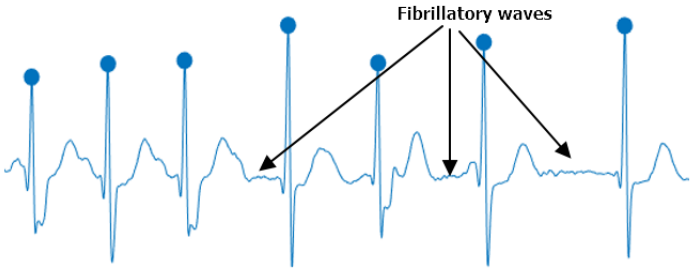

Figure 2.4: Waveform of an AF ECG signal from a real patient. The blue dots mark R peaks.

Since multiple waves exist in a single beat of an ECG of recording, the spectrum of ECG consists of various frequency components. A typical short-term ECG power spectral density (PSD) is shown in Fig. 2.5. These peaks in the figure correspond to different waves [21]:

- The peak at 1 Hz represents the heart rate (60bpm)
- The peak at 4 Hz corresponds to the T-wave
- The peak at 7 Hz means the frequency of P-wave.
- The peak at 10 Hz represents the QRS complex.

Although these particular numbers vary across patients, leads, and body conditions, the order of them does not change. Since AF happens in the atrium, P-waves are more important in this sense. P-waves have a narrow frequency band ranging from 0 Hz to 15 Hz [22].

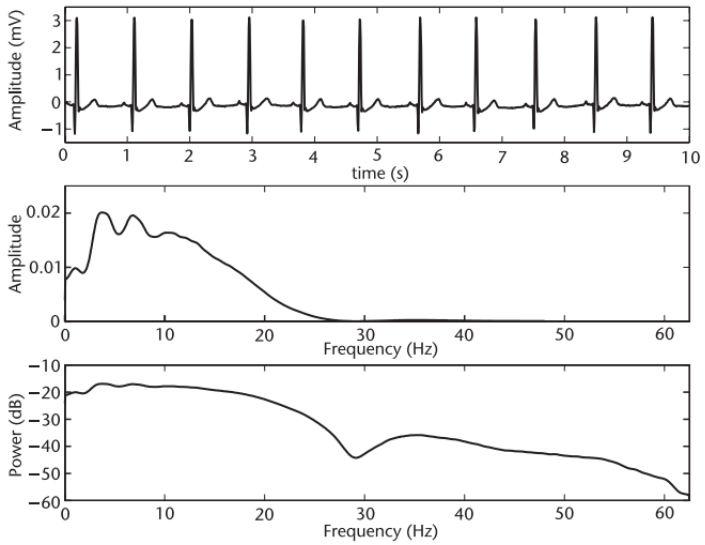

Figure 2.5: A typical PSD of ECG. Source: [21]

2.4 AR & ARMA Modeling

To obtain interpretable information from the heart, one option is to implement parametric models to model the ECG signal or the components of the ECG signal. This section will discuss two types of parametric models that are powerful in dealing with time series: the AR model and the ARMA model. The definition and basic equations will be given. The relationship between the AR model and the linear prediction coding will be discussed following the conception of the AR model, which makes it possible for the AR model to extract the formant. At the end of the section, the applications of the AR model in ECG will be discussed.

2.4.1 Basic Concept of AR model

The AR model is a commonly-used model in dealing with time series. It holds the assumption that the target process is a so-called autoregressive process, meaning that the present sample in a series can be predicted by the weighted sum of previous samples with an uncorrelated Gaussian distributed error. Due to this special property, this model has been used in multiple domains like signal processing, econometrics prediction, and statistics [23]. In the signal processing domain, it plays a crucial role in biomedical signal processing, speech signal processing, and signal encoding [24]. The literature on the AR model on the ECG signal will be discussed in Section. 2.4.4. In the speech signal processing domain, it is used as the linear predictor estimating the values of each sample by using previous samples and is known as the linear prediction model. The equation of the model is expressed as

$$x_t = \sum_{i=1}^{p} a_i x_{t-i} + \epsilon_t, \tag{2.1}$$

where p is the order of AR model, a_i is the parameter called coefficient, and ϵ_t is white noise. The interpretability means human can easily understand the information and explanation provided by the model. As for the AR model, AR parameters can be interpreted in some manners and allow the information of the input process to be understood easily. Hence, the AR model is a parametric model and interpretable. By using the lag operator to represent the lag, the equation can be rewritten as

$$x_t = \sum_{i=1}^{p} a_i L^i x_t + \epsilon_t, \tag{2.2}$$

and this can be further written as the below equation by shifting the summation to the left side, where $a_0 = 1$.

$$\sum_{i=0}^{p} a_i L^i x_t = \epsilon_t. \tag{2.3}$$

In this case, an AR model can be considered as an output of a linear infinite impulse filter with white noises as the input since ϵ_t is white noise. In addition, Eq. 2.4 gives

the frequency domain description,

$$A(z)X_z = \varepsilon_z. \tag{2.4}$$

where $A(z)$ is specified by

$$A(z) = (1 + a_1 z^{-1} + a_2 z^{-2} + \cdots + a_p z^{-p}) \tag{2.5}$$

In this case, the AR coefficients compose a filter $A(z)$ where the input is the time series and the output is the white noise. Since the input process is correlated and the output white noise is uncorrelated, it is easy to understand that this model has the capability of decorrelating. This is why it is implemented in the thesis: to exploit its decorrelation property, the P-waves can be modeled as a pulse train activating the atrium.

Since the AR model is parametric, the way to compute the coefficients is pretty important. The simplest way to achieve that is to minimize the minimum squared error (MSE):

$$\begin{aligned} \mathbf{a} &= \arg\min E[(x_t - a_0 - a_1 x_{t-1} - \cdots - a_p x_{t-p})]^2 \\ \mathbf{a} &= [a_0, a_1, \ldots, a_p]^T \\ a_0 &= (1 - a_1 - \cdots - a_p)\mu. \end{aligned} \tag{2.6}$$

However, the MSE method is not robust since it may lead to the wrong source signal because the minimum value might correspond to another source signal [25]. In real cases, there are other methods used to reach these coefficients, which are more stable and will be introduced in the following Chapters.

2.4.2 AR Model and Linear Prediction Coding

The AR model belongs to linear prediction coding (LPC) in the speech signal domain [26]. LPC is one of the most powerful and parametric speech analysis methods [27, 28]. Its application in speech signal processing provides the intuition of this thesis, which will be introduced in this section. It is used to model the human speech production system. The idea is expressed in Fig. 2.6.

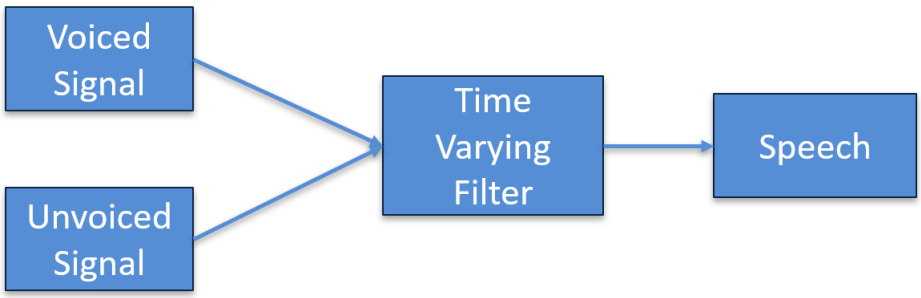

Figure 2.6: The diagram of the LPC filter applied on speech processing.

The voiced signal and unvoiced signal compose the excitation signal, where the voiced signal is an impulse train. The time-varying filter is LPC, representing the combination

of spectral contributions by the glottal flow, the voice tract, and the radiation of lips. The system function of it is given by

$$H(z) = \frac{S(z)}{X(z)} = \frac{G(1 - \sum_{j=1}^{M} b_j z^{-1})}{1 - \sum_{i=1}^{N} a_i z^{-i}}, \tag{2.7}$$

where G is the gain. If the order of the denominator is high enough, this state system function can be approximated by an all-pole filter [26],

$$H(z) = \frac{G}{A(z)} = \frac{G}{1 - \sum_{i=1}^{p} a_i z^{-i}}, \tag{2.8}$$

and the temporal expression is

$$s_n = Gx_n + \sum_{j=1}^{p} a_j s_{n-j}. \tag{2.9}$$

Therefore, it becomes the AR model. It can be understood that the AR model is a special case of the LPC.

The LPC, or the AR model, is often used to model the vocal tract characterized by resonances. These resonances give rise to the formants in the frequency spectrum: behaving as some peaks in the spectrum [29]. In fact, a formant represents the concentration of the energy around a specific resonance frequency in the speech signal. In other words, the LPC or AR model can tell the information about the vocal resonance property. Therefore, the parameters from this parametric model are of spectral interpretability related to the vocal tract.

2.4.3 ARMA model

The autoregressive moving average (ARMA) model is another well-known method to investigate the time series in the statistical sense. With the prerequisite that the input process is stationary, the ARMA model consists of an AR term and a moving average term [30]. Compared to the AR model, the moving average term is introduced to model the error term as a linear combination of values of the present and past errors. The ARMA model is written as $ARMA(p, q)$ and the formula is expressed as

$$x_t = \sum_{i=1}^{p} a_i x_{t-i} + \sum_{j=1}^{q} b_j \epsilon_{t-j} + \epsilon_t, \tag{2.10}$$

where p is the order of the AR term, q is the order of the moving average term, and ϵ_i is the error term following identical independent and identically distributed white noise.

The advantage of the ARMA model is it can achieve the same decorrelation performance as the AR model but uses fewer orders. That is, it can replace the AR model by using fewer poles and introducing some zeros. In this case, the ARMA model can be a more parsimonious choice when dealing with some underlying process. The disadvantage of

it is the longer length requirement for the input. In principle, the AR model at least needs a series with the length of p. However, the ARMA model requires at least pq observations to do backcasting and $p + q + 1$ samples to compute the initial guess. Hence, the least length of the process required by ARMA model is $max(p + q + 1, pq)$ Besides, the choice of q is critical because the ARMA model is not invertibe in some cases.

As mentioned above, the prior condition that the ARMA model holds is that the process is stationary. In the case where the input process is not stationary, the series should be differentiated to become stationary prior to entering into the model. This is because the differentiation can help stabilize the mean of the process by removing the time-dependent changes.

2.4.4 AR Modeling in ECG

The AR model is widely-used in ECG signal processing. In this section, two applications are introduced.

Firstly, the AR model can be used to extract components of ECG signals like f-waves [17, 25, 31]. In this case, the f-waves are modeled as an AR process and the aim is to separate the atrial source from the combination of sources of atrial, ventricular, and extracardiac origin. To connect this problem with the AR model, the linear model is firstly written as

$$\mathbf{x}(n) = \mathbf{A}\mathbf{s}(n), \tag{2.11}$$

where $\mathbf{A}$ is $L \times L$ instantaneous unknown mixing matrix, and $\mathbf{s}(n)$ contain the signals from L different 'sources'. $\mathbf{x}(n)$ represents ECG signals from L leads and are prewhitened. In this case, Eq. 2.11 is formulated in the array processing form. In the context of extraction of f-waves, $s_1(n)$ is assumed to be the atrial source, i.e., the f-wave source. Hence, the aim becomes to recover $s_1(n)$ from $\mathbf{x}(n)$:

$$d(n) = s_1(n) = \mathbf{w}^T\mathbf{x}(n), \tag{2.12}$$

where $\mathbf{w}$ is demixing vector and $\mathbf{w}^T\mathbf{w} = 1$. The demixed signal $d(n)$ is modeled as an AR process,

$$\hat{d}(n) = \sum_{p=1}^{P} a_p d(n-p). \tag{2.13}$$

The prediction error is expressed as

$$e_d(n) = d(n) - \hat{d}(n), \tag{2.14}$$

and this can be further derived as

$$e_d(n) = \mathbf{w}^T(\mathbf{x}(n) - \sum_{p=1}^{P} a_p\mathbf{x}(n-p)) = \mathbf{w}^T\mathbf{e}_x(n), \tag{2.15}$$

In this case, $\mathbf{w}$ can be obtained by minimizing the mean square error ,

$$E[e_d^2(n)] = \mathbf{w}^T E[\mathbf{e}_x(n)\mathbf{e}_x^T(n)]\mathbf{w}, \tag{2.16}$$

subject to $\mathbf{w}^T\mathbf{w} = 1$.

The second application is to exploit AR coefficients for classification [32–34]. In this application, the AR model is implemented to extract features of ECG signals in SR and arrhythmia cases. Then, some classification techniques are used, most of which are machine learning algorithms [33, 34]. This literature achieved high accuracy of classification by exploiting machine learning algorithms. Nevertheless, the drawback of machine learning is accompanied. That is, the interpretability is weak. For instance, [33] uses the generalized linear model which uses the Euclidean distance between AR parameters, but no interpretations of the parameters were explored. As a result, these papers did not explore the physiological relationship between AR coefficients and ECG signals.

2.5 Problem Formulation

Among these works of literature using the AR model described above, the whole ECG signals are processed. Whereas it is possible to obtain information related to the AF only based on P-waves and f-waves due to that P-waves reflect the atrium activities and AF happens due to atrium dysfunction. Hence, in this thesis, we focus on P-waves and extract them first.

Similar to the idea of how the AR model models the vocal tract, as introduced in Section.2.4.2, the idea is to use the AR model to model the atrium. This is because of a similar mechanism from the signal processing perspective: both inputs of the vocal tract and the atrium can be considered as impulse trains. Fig. 2.7 illustrates this idea, where schematic diagrams of the pulse train and P-waves are drawn. In this diagram, the pulse train representing the voiced signal in Fig. 2.6 becomes the pulse train from the SA node. The output speech signal now turns to P-waves. In other words, the SA node sends pulse trains in nature, and the atrium is modeled as an AR model.

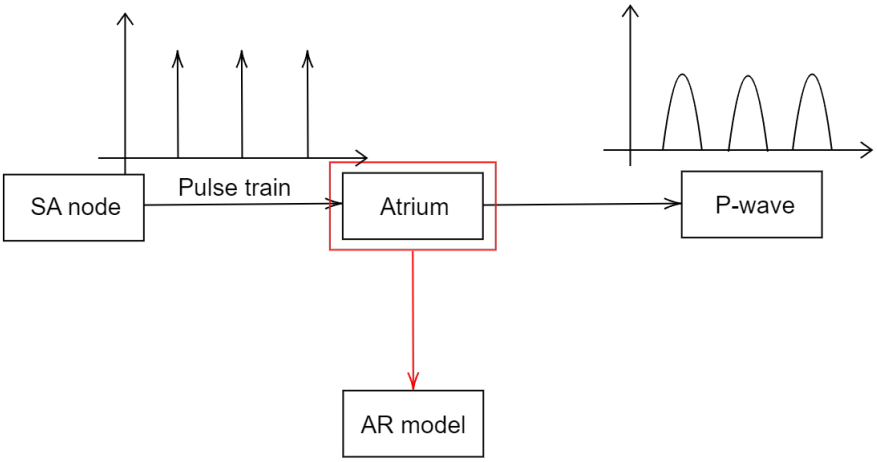

Figure 2.7: The flowchart of the idea.

Hence, it can be expected that the AR model can yield the information in a similar manner as the LPC does in the vocal tract. This kind of information in the SR case and AF case can be compared and analyzed, such as changes in the atrium in the AF case. Moreover, the ARMA model is also applied and the comparison is made. The classification is done based on the extracted information, which will be introduced in the following Chapters.

3 Proposed Atrium AR Model

This chapter introduces the first contribution of this thesis: building the atrium model, including the preprocessing block and the atrium modeling block in Fig. 1.1. The extraction of P-waves, which corresponds to the preprocessing block, will be discussed in Section. 3.1.2, including noise reduction and P-waves delineation. After P-waves are extracted, the following model needs to be built. The pre-requisition of the AR model and ARMA model is the stationarity of the input process. Therefore, the stationarity will be assessed quantitatively in Section. 3.2. Afterward, the methods to compute the AR model and ARMA model are discussed in Section. 3.3 and Section. 3.4. Section. 3.5 will illustrate the order identification and quantify the correlation removal of these two models, allowing to determine the final model. Last, Section. 3.6 will present the implementation, some results, and discussions of signals.

3.1 Extraction of P waves

As discussed in Chapter 2, P-waves are the input of the model due to the fact that AF mainly influences the atrium. In this case, it is necessary to extract P-waves at first. In this section, the technique of P-waves acquisition will be discussed, including noise reduction and P-waves delineation.

3.1.1 Noise Reduction

Real ECG signals are always incorporated with many noises and artifacts. There are three types of noises influencing the modeling performance of ECG signal: the baseline wander (BLW), powerline interference, noises caused by muscle activities, and electrode motion artifacts [35]. Besides, there is another common noise that exists in all real ECG recordings used and is discovered in the experiments.

The BLW, also known as baseline drift, is the effect where the base of the ECG signal moves up and down instead of being orderly. In this case, the signal is shifted away from the baseline. The frequency of BLW ranges from $0 - 0.5$ Hz which is a very low frequency band. Hence, a high-pass filter with a cut-off frequency of 0.6 Hz can remove it. In this thesis, the zero-phase fourth-order Butterworth filter is used as a high-pass filter. The Butterworth filter is one of the most commonly used frequency domain filters due to its sharp frequency roll-off feature [36]. The frequency response is expressed as

$$|H(w)|^2 = \frac{1}{1 + (\frac{\omega}{\omega_c})^{2n}} \tag{3.1}$$

where ω is the frequency, ω_c is the cut-off frequency, and n is the filter order. An example is shown in Fig. 3.1. The signal is a simulated ECG signal only containing BLW artifacts. Fig. 3.1 shows the filtered signal is lined up well, meaning that BLW artifacts can be removed by the designed filter effectively. What is noticeable is that though removing BLW, the base amplitude of the signal is a negative value instead of zero.

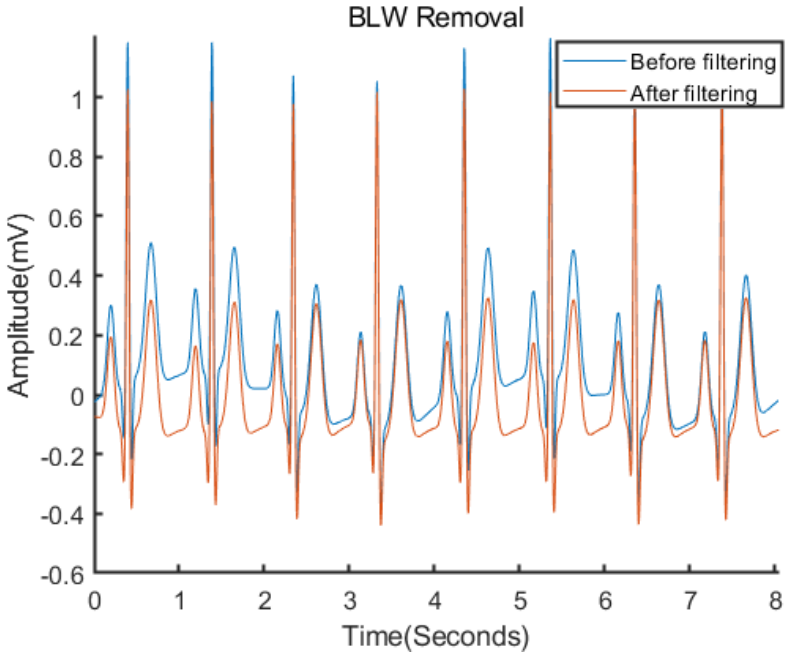

Figure 3.1: Comparison between the signal before removing BLW and after when the input is a simulated ECG signal. The filter at 0.6 Hz can filter the BLW artifacts well such that the resulting signal is lined up.

Powerline interference is an instrumental noise, originating from electromagnetic interference of the alternating supply [37]. It performs as interference at the frequency of 50 Hz or 60 Hz, where a peak appears at the spectrum. This interference makes it difficult for ECG analysis since it contaminates low-amplitude components like T waves and P waves. Since its typical frequency is 50 Hz, the low-pass filter with a cut-off frequency of 50 Hz can be used to reduce it. Fig. 3.2 shows an example of noise reduction where the signal is a real ECG signal. It shows the powerline interference is reduced drastically.

Muscle noise is caused by muscle activities during measuring ECG signals. In contrast to the previous two types of noises, this kind of noise can not be removed easily, and the technique to reduce it is still underdeveloped [35]. It is because its frequency spectrum overlaps the whole ECG spectrum. But normally, this noise only appears several beats and hence it will not impose a big influence on the results of the thesis. A real ECG containing this noise is plotted in Fig. 3.3, where the muscle noise is shown in the red rectangle.

In the experiments, another low-frequency noise is found in real ECG recordings from the SR dataset which is the MIT-BIH normal sinus rhythm dataset [38], which does

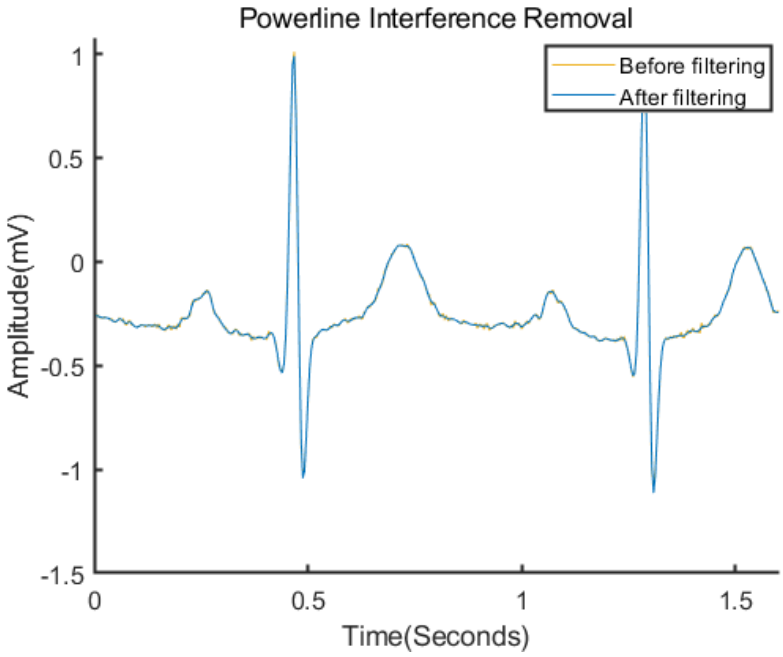

Figure 3.2: Comparison between the signal before removing powerline interference and after. The signal is a real ECG signal. It shows the powerline interference depicted in yellow is removed.

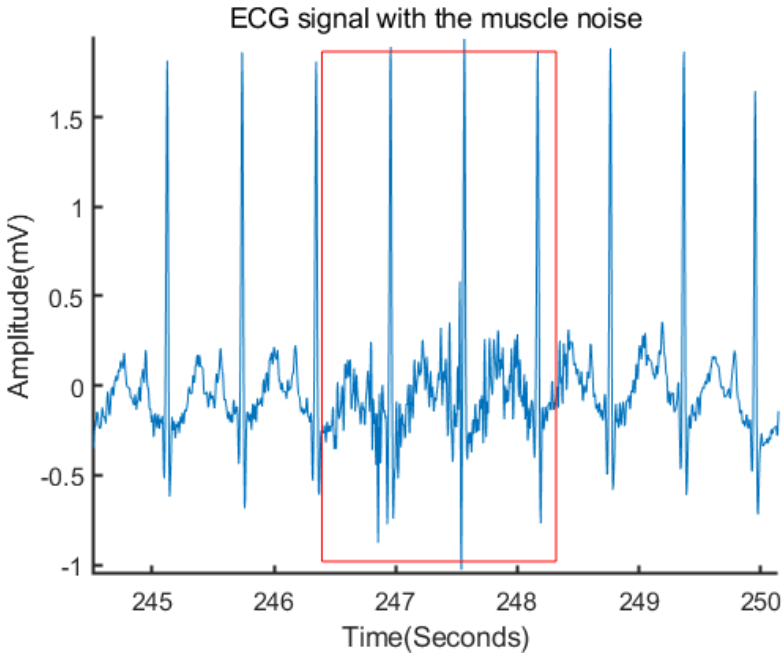

Figure 3.3: A real ECG signal contains the muscle noise that is encircled by the red rectangle. This kind of noise only happens in a short time duration, normally several beats.

not belong to any of the types of noises mentioned in [35]. This special noise made it difficult for the model to model the atrium activities since the P-waves are also low-frequency and noises and P-waves are mixing. To elaborate on the noises, some real ECG signals will be considered. But firstly, a series of P-waves extracted from a simulated ECG signal will be used to describe the true PSD of the P-waves. The waveform and the PSD are shown in Fig. 3.4. According to (b) in Fig. 3.4, the most energy of P-waves concentrates at around 5 Hz, which means a peak envelope, i.e., only one formant, appears there. In addition, no very low-frequency peak emerges here.

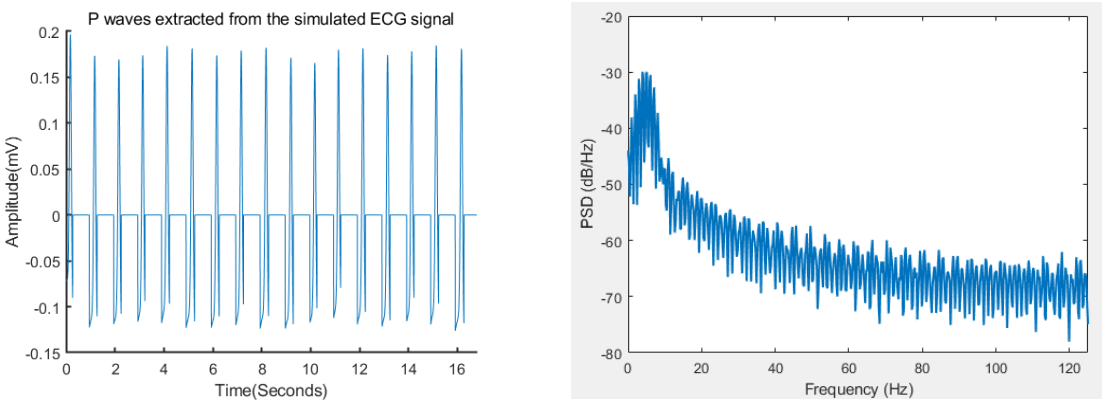

(a) Simulated P-waves

(b) PSD of simulated P-waves

Figure 3.4: Simulated P waves and the PSD. A formant can be observed in the PSD around 5 Hz.

Then, for real noisy recordings whose P waves are not prominent, the peak of P waves will become lower than the low-frequency noise peak. Since there are too many recordings in the SR dataset and it is not possible to show them all, only the first four recordings are used as examples to explain this noise, and their PSDs are shown in Fig. 3.5. Among them, one recording has prominent P-waves and it's PSD is shown in (a) in Fig. 3.5. The others have weaker P-waves that are overwhelmed by low-frequency noises and their PSDs are depicted in (b)-(d). It can be observed that a common peak at a frequency around 1.2 Hz arises in all PSDs except recording in (a). Instead, the PSD in (a) shows the most energy at around 10 Hz, whose morphology matches the normal situation, i.e., the simulated P-waves. The conditions of subjects of these recordings can not be known in detail at the present time because the public SR dataset has been constructed since the 1990s and no detailed information about how recordings were made is given. However, by observing signal waveforms, it is discovered that such kind of noise exists in the recordings which are noisy and have weak P-waves amplitude. Moreover, both the simulated P-waves and clean P-waves perform only one formant instead of two. In this noisy case, the peak which represents the most energy of P-waves is weaker than the noise peak around 1.2 Hz, like the peak at around 8 Hz in (b). This kind of low-frequency noise will do harms to the information extraction based on P-waves because the AR model focuses on modeling signals from the frequency perspective. In order to overcome the low-frequency noise, the cut-off frequency of 0.6 Hz of the high-pass filter used to remove BLW is extended to 1.3 Hz

such that this noise at around 1.2 Hz can be filtered.

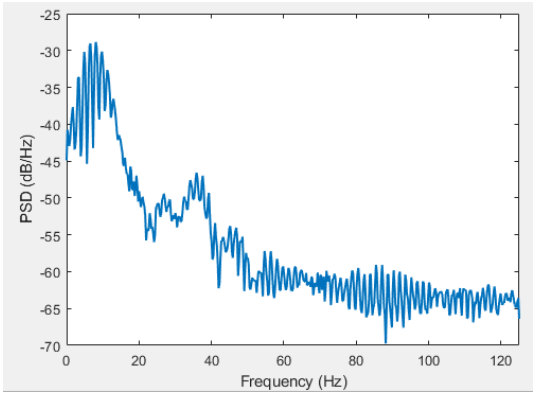

(a) PSD of the real P-waves from the recording which has prominent P-waves and little noises.

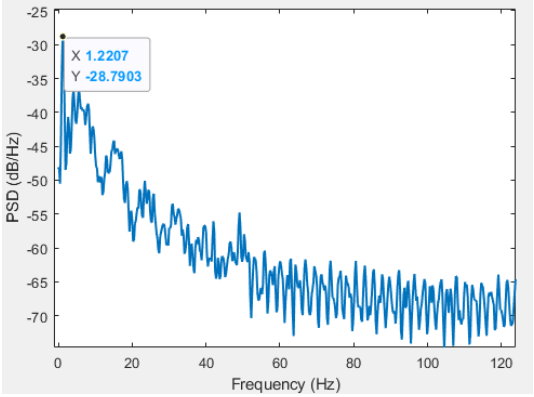

(b) PSD of the real P-waves from the recording when P-waves are weak and noises are prominent.

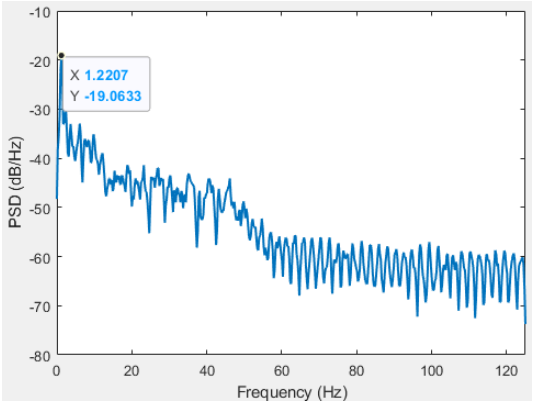

(c) PSD of the real P-waves from another noisy recording.

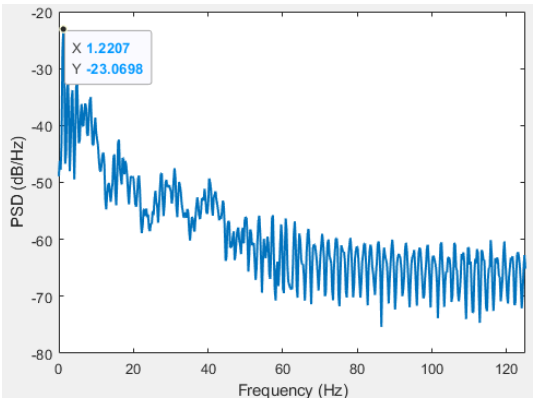

(d) PSD of the real P-waves from another recording.

Figure 3.5: PSD of real P-waves. (a) depicts the recording which is pretty clean and has prominent P-waves. (b)-(d) plots recordings with prominent low-frequency noises and weak P-waves

It has to be mentioned that the cut-off frequency of 1.3 Hz will also remove some content of P-waves, but most energy of P-waves remains and it really improves the results that will be shown in the following chapters. Otherwise, the information of P-waves will be masked by low-frequency noises.

3.1.2 Wave Extraction

A preliminary step for modeling P-waves is to delineate P-waves from the raw ECG signal. An open-source detector is used to identify the R peaks in the ECG [38, 39]. It is developed based on the envelop detecting method to achieve the information related to R peaks and RR intervals [40–42]. After obtaining the locations of R peaks, the QRST complexes should be removed afterward such that only P-waves are preserved. To achieve this goal, a rectangular window is used. Then, the QRST complexes are

subtracted from the ECG signal and hence P waves remain. The window is built based on these detected R peaks,

$$\begin{aligned} start &= R_{peak} - 0.1 * T \\ end &= R_{peak} + 0.7 * T \end{aligned} \tag{3.2}$$

where R_{peak} denotes the location of an R peak. The length of a window is characterized by the window length parameter T that depends on the type of window length. There are two types of window length developed: the minimum window length (MWL) method and the average window length (AWL) method. For MWL, T is defined as the minimum RR interval, and T is considered the average RR interval for AWL,

$$\begin{aligned} MWL: &\quad T = min\{RRinterval\} \\ AWL: &\quad T = avg\{RRinterval\} \end{aligned} \tag{3.3}$$

.

When dealing with SR ECG signals, the different T does not make much difference. It is because the normal ECG signal is regular, and hence the minimum RR interval and the average of RR intervals are not different in principle. However, when dealing with the AF signals, AWL and MWL methods will have large differences in the window due to the irregular RR intervals. If using the MWL method, some other components, like T waves, are not subtracted and will remain in the extracted signal. This will influence the following modeling. An example is shown in Fig. 3.6. This problem happens due to the irregularity of AF which causes some RR intervals to become pretty small. If such an RR interval is picked as the window length, it is not representative of the whole signal.

To address this problem, the AWL is considered and residual T waves can be excluded. However, although the extra components are eliminated, some f-waves are not extracted due to irregularity. For very small R-R intervals, the window located at the first QRST complex will overlap with the window of the second QRST complex. In this case, f-waves in this R-R interval will be omitted. An example of the extracted AF signal illustrating this problem is shown in Fig. 3.7, which is extracted from the same signal as Fig. 3.6. This figure shows that only f-waves are extracted and no other components remain. The red, green, and pink windows encircle three successive QRST complexes with two small R-R intervals. In these two intervals, three windows cover the two R-R intervals exactly; hence, no f-waves are extracted in these two R-R intervals.

These two windows actually hold different tolerances of errors: the MWL tolerates the disturbances and noises, while the AWL gives tolerance to the missing of data. They will cause different classification performances which will be discussed in Chapter 5.3.

3.2 Stationarity Assessment

AR requires the input signal to be a stationary process. However, a long-term ECG recording is not stationary at all. To guarantee the prerequisite, the ECG signal is usually divided into short windows, which contain $10 - 20$ seconds. In this case, the

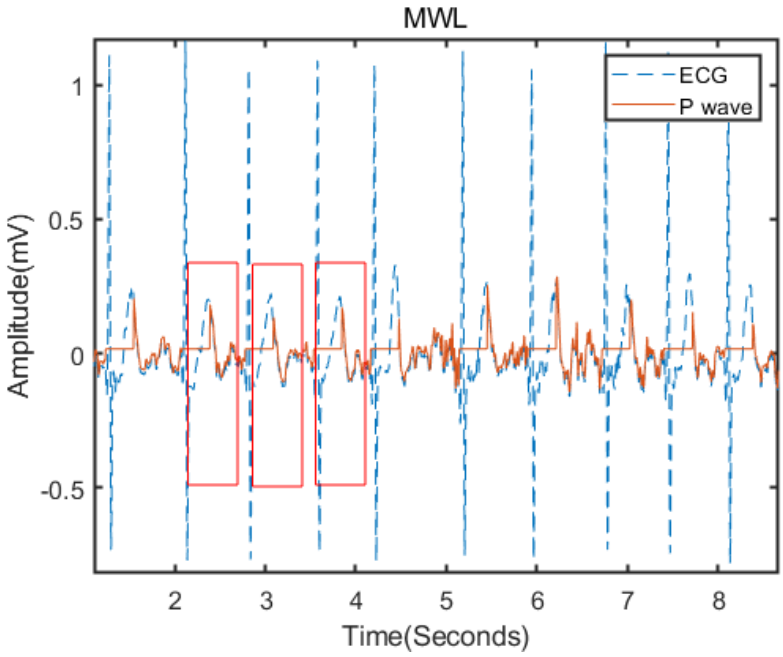

Figure 3.6: Signal extracted from a real recording by using MWL. Red rectangular encircle some residual T waves.

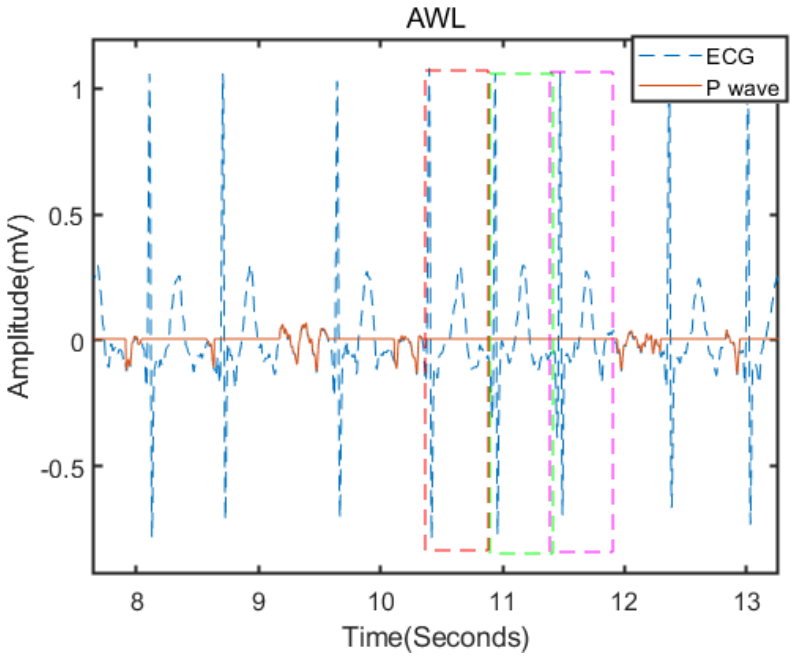

Figure 3.7: Signal extracted from a real recording by using AWL. Three rectangular mark successive small RR intervals in different colors. In these two intervals, three windows cover the two R-R intervals exactly; hence, no f-waves are extracted in these two R-R intervals.

short stationarity assumption can be used, which means the statistical properties of each window can be assumed relatively constant [43, 44]. In this thesis, the P-wave series extracted from the complete ECG signal is divided into 10 equal-length windows, where each window contains around 20 beats. In this case, the length of each window is $15 - 20$ seconds, depending on the heart rate of patients. One problem of direct windowing and dividing is the first beat and the last beat of the recording may not contain intact components, i.e., these two beats only have T-wave or half of QRS complexes. To address this problem, the first and last beats are discarded.

Although windowed signals hold the short stationarity assumption intuitively, it is good to prove and quantify the stationarity. The augmented Dickey-Fuller (ADF) test is implemented in order to achieve this. In other words, it tells whether a signal is stationary or not [45]. This test is done based on the so-called unit root representing the random walks of the process. The unit root is defined by the one value of a_1 in the equation of the AR model: if there is a parameter $|a_1| = 1$, the unit root exists. It describes the random walks of the process in the statistical sense. Hence, a process with a unit root is considered non-stationary. In addition, ADF test is based on the hypothesis that the unit root is present in the time series. It is conducted with two assumptions:

- Null hypothesis: The series is non-stationary, and it has a unit root.
- Alternative hypothesis: the series is stationary, and it does not have a unit root.

For the null hypothesis, the formula is written as

$$x_t = x_{t-1} + \beta_1 \Delta x_{t-1} + \beta_2 \Delta x_{t-2} + \cdots + \beta_p \Delta x_{t-p} + \epsilon_t \tag{3.4}$$

where a_1 is restricted to 1, and Δ represents the differencing operator. In this case, the differences of the series are introduced compared with the original formula of the AR model. This is done by adding and subtracting $a_{i+1}x_{t-i}$:

$$x_t = x_{i-1} + \cdots + (a_i + a_{i+1})x_{t-i} + a_{i+1}(x_{t-i} - x_{t-(i+1)}) + \cdots + a_p x_p + \epsilon_t \tag{3.5}$$

and

$$x_t = x_{i-1} + \cdots + (a_i + a_{i+1})x_{t-i} + a_{i+1}\Delta x_{t-i} + \cdots + a_p x_p + \epsilon_t \tag{3.6}$$

where $a_{i+1} = \beta_i$. This adding-and-subtracting step is done recursively, and Eq. (3.4) can be obtained. As for the alternative hypothesis, the model is

$$x_t = a_1 x_{t-1} + \beta_1 \Delta x_{t-1} + \beta_2 \Delta x_{t-2} + \cdots + \beta_p \Delta x_{t-p} + \epsilon_t \tag{3.7}$$

where $a_1 < 1$. The estimate $\hat{a}_1$ is solved by linear regression with the help of QR decomposition. The test statistic used is standard $\mathbf{t}$ statistic, i.e.,

$$t_1 = \frac{\hat{a}_1 - 1}{SE(\hat{a}_1)} \tag{3.8}$$

where $\hat{a_1}$ is the ordinary least squares estimate of a_1 and $SE(\hat{a_1})$ is the standard error in the alternative model. Finally, the test tells the confidence of the presence of the unit root by computing the cumulative distribution function of t_1.

3.3 AR Coefficient Computation

Although the coefficients of the AR model can be computed easily by the LSE method mentioned in Chapter. 2.5, it is more stable to use other methods like the Yule-Walker method or the Burg method to obtain the coefficients. In this section, these two methods will be implemented and discussed.

3.3.1 Yule-Walker Method

The Yule-Walker method is common when it comes to computing the coefficients of the AR model. This method is based on solving Yule-Walker equations [46]. Recall the formula of the AR model

$$x_t = \sum_{i=1}^{p} a_i x_{t-i} + \epsilon_t \tag{3.9}$$

If x_{t-k} (the sample at lag k) is multiplied to both sides in Eq. (3.9), the equation becomes

$$x_{t-k}x_t = \sum_{i=1}^{p} a_i x_{t-i}x_{t-k} + \epsilon_t x_{t-k} \tag{3.10}$$

and take the expectance,

$$E(x_{t-k}x_t) = \sum_{i=1}^{p} E(a_i x_{t-i}x_{t-k}) + E(\epsilon_t x_{t-k}) \tag{3.11}$$

If the noise at the present time is uncorrelated with the previous values of the signal, the zero correlation term can be eliminated,

$$E(x_{t-k}x_t) = \sum_{i=1}^{p} E(a_i x_{t-i}x_{t-k}) \tag{3.12}$$

where $E(x_{t-k}x_t)$ is the covariance between x_t and itself at lag k, i,e, autocovariance. Using c_k to represent it and exploiting the evenness of autocovariance that $c_k = c_{-k}$, the previous equation can be expressed as

$$c_k = \sum_{i=1}^{p} a_i c_{i-k} \tag{3.13}$$

Divide through by c_0,

$$\rho_k = \sum_{i=1}^{p} a_i \rho_{i-k} \tag{3.14}$$

where ρ_k is the Pearson correlation coefficient [47]. Eq. (3.14) is general since k can be any number other than 0. Collecting equations at all lags together and stacking them

can yield

$$\begin{aligned}
\rho_1 &= \sum_{i=1}^{p} a_i \rho_{i-1} \\
\rho_2 &= \sum_{i=1}^{p} a_i \rho_{i-2} \\
&\cdots \\
\rho_p &= \sum_{i=1}^{p} a_i \rho_{i-p}
\end{aligned} \tag{3.15}$$

$$\begin{bmatrix} \rho_1 \\ \rho_2 \\ \cdots \\ \rho_p \end{bmatrix} = \begin{bmatrix} \rho_0 & \rho_1 & \cdots & \rho_{p-1} \\ \rho_1 & \rho_0 & \cdots & \rho_{p-2} \\ \vdots & & & \vdots \\ \rho_{p-1} & \rho_{p-2} & \cdots & \rho_0 \end{bmatrix} \begin{bmatrix} a_1 \\ a_2 \\ \cdots \\ a_p \end{bmatrix} \tag{3.16}$$

$$\underbrace{\begin{bmatrix} \rho_1 \\ \rho_2 \\ \vdots \\ \rho_p \end{bmatrix}}_{\mathbf{r}} = \underbrace{\begin{bmatrix} \rho_0 & \rho_1 & \cdots & \rho_{p-1} \\ \rho_1 & \rho_0 & \vdots & \rho_{p-2} \\ \vdots & \cdots & & \cdots \\ \rho_{p-1} & \cdots & \vdots & \rho_0 \end{bmatrix}}_{\mathbf{R}} \underbrace{\begin{bmatrix} a_1 \\ a_2 \\ \vdots \\ a_p \end{bmatrix}}_{\mathbf{a}}$$

In this case,

$$\mathbf{r} = \mathbf{R}\mathbf{a} \tag{3.17}$$

since $\rho_0 = 1$, $\mathbf{R}$ have diagonal elements of 1. It means $\mathbf{R}$ is full rank and symmetric. Hence, it is invertible and the coefficients can be solved

$$\hat{\mathbf{a}} = \mathbf{R}^{-1}\mathbf{r}. \tag{3.18}$$

The Levinson–Durbin algorithm is often used to solve this equation at a faster computer speed, which is a recursion algorithm [48, 49].

3.3.2 Burg Method

Burg method is another method to estimate coefficients $\mathbf{a}$ robustly in a forward-and-backward prediction manner. Instead of computing coefficients directly, the Burg method estimates reflection coefficients that measure the correlation between two samples [50]. To be specific, the reflection coefficient k_p measures the correlation between x_t and x_{t-n} by ignoring the influences of samples at all other lags. The $-k_p$ is the partial autocorrelation. The Burg method first computes the forward and backward

prediction errors, which are defined as

$$\begin{aligned} e_{f,p}(t) &= x(t) + \sum_{i=1}^{p} a_{p,i} x(t-i), \quad t = p+1, \ldots, N \\ e_{b,p}(t) &= x(t-p) + \sum_{i=1}^{p} a^*_{p,i} x(t-p+i), \quad t = p+1, \ldots, N, \end{aligned} \tag{3.19}$$

where p indicates the order. Since there are too many subscripts, the x_t is written as $x(t)$. The AR coefficients are determined by

$$a_{p,i} = \begin{cases} a_{p-1,i} + k_p a^*_{p-1,p-i}, & i = 1, \ldots, p-1 \\ k_p, & i = p. \end{cases} \tag{3.20}$$

The k_p in the Burg method is obtained by minimizing the mean of two prediction error variances,

$$\min_{\hat{k}_p} \frac{1}{2}[\rho_f(p) + \rho_b(p)], \tag{3.21}$$

where

$$\begin{aligned} \rho_f(p) &= \frac{1}{N-p} \sum_{t=p+1}^{N} |e_{f,p}(t)|^2 \\ \rho_b(p) &= \frac{1}{N-p} \sum_{t=p+1}^{N} |e_{b,p}(t)|^2. \end{aligned} \tag{3.22}$$

With these equations, Eq. 3.19 can be further expressed as

$$\begin{aligned} e_{f,p}(t) &= e_{f,p-1}(t) + k_p e_{b,p-1}(t-1) \\ e_{b,p}(t) &= e_{b,p-1}(t-1) + k^*_p e_{f,p-1}(t). \end{aligned} \tag{3.23}$$

Since Eq. 3.21 is actually quadratic in k_p, according to [48], k_p can be obtained by

$$k_p = \frac{-2 \sum_{t=p+1}^{N} e_{f,p}(t) e^*_{b,p}(t-1)}{\sum_{t=p+1}^{N} [|e_{f,p}(t)|^2 + |e_{b,p}(t-1)|^2]}. \tag{3.24}$$

In this case, the recursive Burg algorithm is listed in Algorithm. 1

3.4 ARMA Coefficient Computation

As for the computation of ARMA coefficients, it is not as trivial as the AR model due to the introduced MA coefficients which make the estimation nonlinear. The conditioned maximum likelihood estimation (MLE) is implemented to solve this problem [51–53]. All coefficients in Eq. (2.10) can be collected to a set of parameters

$$\theta^T = (a_1, \ldots, a_p, b_1, \ldots, b_q). \tag{3.25}$$

Algorithm 1 The Burg algorithm

1: Initialization: $e_{f,0}(t) = e_{b,0}(t) = x(t), \quad m = 1$
2: **repeat**
3: $\quad e_{f,m}(t) = e_{f,m-1}(t) + k_m e_{b,m-1}(t-1)$
4: $\quad e_{b,m}(t) = e_{b,m-1}(t-1) + k_m^* e_{f,m-1}(t)$
5: $\quad k_m = \frac{-2\sum_{t=m+1}^{N} e_{f,m}(t) e_{b,m}^*(t-1)}{\sum_{t=m+1}^{N}[|e_{f,m}(t)|^2 + |e_{b,m}(t-1)|^2]}$
6: $\quad a_{m,i} = \begin{cases} a_{m-1,i} + k_m a_{m-1,m-i}^*, & i = 1, \ldots, m-1 \\ k_m, & i = m. \end{cases}$
7: $\quad m \leftarrow m + 1$
8: **until** $m = p$

Output: **a**, **k**

Then, the likelihood function of $\mathbf{x}$ is written as

$$L(\mathbf{x}_t; \theta, \sigma_\epsilon^2) = f(\mathbf{x}_t | \theta, \sigma_\epsilon^2), \tag{3.26}$$

where

$$\mathbf{x}_t^T = [x_t, x_{t-1}, \ldots, x_1]. \tag{3.27}$$

Since $x_k, k \in \{t, t-1, \ldots, 2\}$ only depends on ϵ_k given $\mathbf{x}_{k-1}$ and ϵ_k is white noise, the likelihood function can be further derived as

$$f(\mathbf{x}_t | \theta, \sigma_\epsilon^2) = \prod_{i=p+1}^{t} f(x_t | \mathbf{x}_{t-1}, \theta, \sigma_\epsilon^2) f(\mathbf{x}_p | \theta, \sigma_\epsilon^2). \tag{3.28}$$

Set $\epsilon_p = \epsilon_{p-1} = \cdots = \epsilon_{p-q+1} = 0$ to create the conditioned likelihood function [52, 53]. Hence, Eq. (3.28) reduces to

$$f(\mathbf{x}_t | \theta, \sigma_\epsilon^2) = \prod_{i=p+1}^{t} f(x_t | \mathbf{x}_{t-1}, \theta, \sigma_\epsilon^2) \tag{3.29}$$

With the reasonable assumption that the process is Gaussian due to the white noise ϵ_t, then the likelihood function can be expanded,

$$L(\mathbf{x}_t; \theta, \sigma_\epsilon^2) = (\sigma_\epsilon^2 2\pi)^{-\frac{t-p}{2}} exp(-\frac{1}{2\sigma_\epsilon^2} \sum_{k=p+1}^{t} \epsilon_k^2). \tag{3.30}$$

Take the logarithm of Eq. (3.30),

$$\mathcal{L}(\mathbf{x}_t; \theta, \sigma_\epsilon^2) = -\frac{t-p}{2} log(2\pi) - \frac{t-p}{2} log(\sigma_\epsilon^2) - \sum_{k=p+1}^{t} \frac{\epsilon_k^2}{2\sigma_t^2}. \tag{3.31}$$

In this sense, maximizing the log-likelihood becomes minimizing the sum of square errors, i.e., $\sum_{k=p+1}^{t} \frac{\epsilon_k^2}{2\sigma_t^2}$. Denote it as

$$S(\theta) = \sum_{k=p+1}^{t} \epsilon_k^2. \tag{3.32}$$

It is a function of θ since ϵ_k is given by

$$\epsilon_k = x_k - \sum_{i=1}^{p} a_i x_{t-i} - b_1 \epsilon_{k-1} - \cdots - b_q \epsilon_{k-q}. \tag{3.33}$$

By differentiating Eq. (3.31) with respect to σ_ϵ^2, the estimate of σ_ϵ^2 is obtained,

$$\hat{\sigma}_\epsilon^2 = \frac{S(\theta)}{t-p}. \tag{3.34}$$

Inserting it back to Eq. (3.31) yields

$$\mathcal{L}(\mathbf{x}_t; \theta, \sigma_\epsilon^2) = -\frac{t-p}{2} log(S(\theta)) + c. \tag{3.35}$$

where c represents all constants. This shows maximizing the log-likelihood function is actually minimizing $S(\theta)$, and Newton's method is used to reach the appropriate θ.

3.5 Order Identification and Correlation Removal

For a general ARMA model, Eq. (2.10) can be re-expressed as

$$x_t = h(t) * \epsilon_t \tag{3.36}$$

where

$$H(Z) = \mathcal{FFT}(h(t)) = \frac{B(Z)}{A(Z)} = \frac{\sum_{k=1}^{q} b_k z^{-k}}{1 + \sum_{k=1}^{p} a_k z^{-k}}. \tag{3.37}$$

The ARMA reduces to the AR model when $B(Z) = 1$. Hence, the AR model is an all-pole filter, and the ARMA model is a zero-and-pole model.

Considering the assumption made in Chapter. 2.4.4, the pulse train is sent by the SA node and input to the atrium. Since each pulse is sent independently, the pulse train has a spectrum consisting of infinite single pulse spectrums. It means the spectrum of the pulse train is flat, namely, white; hence, it can be considered ϵ_t. In this sense, the AR or ARMA model can be used to decorrelate P-waves x_t, which means the model filters a signal with a non-white spectrum into a signal with a white spectrum. To determine which model is more useful for further experiments, the decorrelating capability of these models should be evaluated.

3.5.1 Order Identification

The order of the AR or ARMA model is critical since it determines the capability of fitting the signal. One way to identify which order for the AR model is the most appropriate is to use the partial correlation function (PACF). It defines the correlation between the present sample and the sample at lag k but excludes samples at all other

lags. A suitable order of an AR model is the first value smaller than the 95% confidence interval [52]. The formula can be written as Eq. (3.38) by following this idea,

$$\phi_{t,t} = \frac{\rho_t - \sum_{k=1}^{t-1} \phi_{t-1,k}\rho_{n-k}}{1 - \sum_{k=1}^{t-1} \phi_{t-1,k}\rho_k} \tag{3.38}$$

The order of the AR process can be determined by the first value below the 95% confidence level of PACF. The bound of 95% confidence level is determined by

$$bound = \frac{z}{\hat{\sigma}} \tag{3.39}$$

where $\hat{\sigma}$ represents the standard error of the PACF, and $z = 1.96$ when using a 95 percent confidence level [54]. According to [55], when the process is assumed to be autoregressive of order p, $\hat{\sigma}$ satisfies

$$\hat{\sigma} \simeq \frac{1}{\sqrt{t}} \tag{3.40}$$

where t is the length of observations. Fig. 3.8 shows that for simulated P-waves the first value below the confidence interval is at the lag of 6, and for the real P-waves, the first value is at the lag of 11. Hence, the appropriate order in different cases is different. Since the desired model needs a general and determined order for all signals, only a rough range of orders from 6 to 12 can be made. In this case, a further order identification procedure is needed, which will be discussed in Section. 3.5.2.

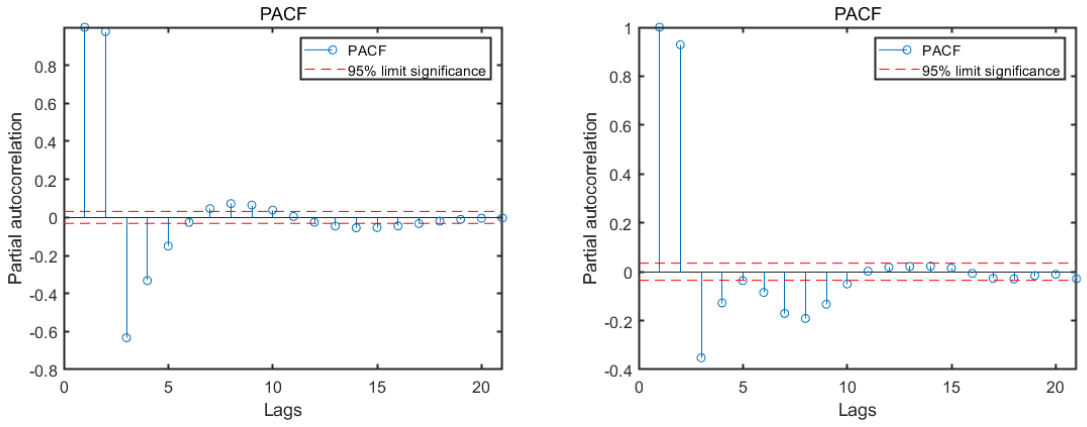

(a) PACF of simulated P-waves within 20 lags. (b) PACF of real P-waves within 20 lags.

Figure 3.8: PACF of simulated and real P-waves.

As for the ARMA model, the Akaike information criterion (AIC) and Bayesian information criterion (BIC) are used to give reference orders of AR and MA terms. AIC and BIC trade off the fitting performance and the model complexity, namely the number of parameters [56, 57]. The algorithm based on AIC and BIC is given in Algorithm. 2, where $p_{max} = 16$, and $q_{max} = 4$. This algorithm of order searching is actually a trial-and-error method. The maximum of q is set to four to guarantee system invertibility.

The initial pair of order is $p_{initial} = 2, q_{initial} = 1$ because the model will become an MA model or AR model if $p = 0$ or $q = 0$. The resulting pair of orders based on simulated P-waves is $p = 10, q = 3$ given by the algorithm.

However, this pair of p, q is too high since the max appropriate order of p of AR model is just 12. The ARMA model eliminates two poles but introduces three zeros. Therefore, AIC and BIC may not give enough useful information in dealing with the P-waves. Under this circumstance, the prediction error variance is considered to evaluate models, which will be discussed in the next part.

Algorithm 2 ARMA Order Identification Algorithm

Input: p_{max}, q_{max}, s
Initialization: $p = 2, q = 1$
repeat
  Estimate ARMA model and obtain L based on p, q, and s
  $q \leftarrow q + 1$
  $p \leftarrow p + 1$
until $p = p_{max}$, $q = q_{max}$
Compute AIC and BIC for each pair of p and q.
$[p_1, q_1] = min\{AIC\}$
$[p_2, q_2] = min\{BIC\}$
$[p_{output}, q_{output}] = min\{p_1^2 + q_1^2, p_2^2 + q_2^2\}$
Output: p_{output}, q_{output}

3.5.2 Correlation Removal

The AR or ARMA model can remove the underlying correlations of the input P-waves. The decorrelated output signal of the model is also called prediction error. The prediction error variance can be used to quantify the remaining correlation in the signal. It is computed by

$$e_t = x_t - \hat{x}_t, \tag{3.41}$$

where $\hat{x}_t$ is the predicted value at the present time and is calculated by

$$\hat{x}_t = -\sum_{i=2}^{p+1} a_i x_{t-i+1}. \tag{3.42}$$

The computation of the prediction error in the AR model is shown in Fig. 3.9. This figure also elaborates on the reason why the prediction error is actually the decorrelated output signal.

The AR model based on the Yule-Walker method, AR model based on the Burg method, and the ARMA models with different numbers of MA terms ranging from 1 to 4 are implemented on simulated and real signals, respectively. The prediction error variances in the AR and ARMA models with different orders of AR terms are shown in the below figures. Fig. 3.10 shows the results based on simulated P-waves, and Fig. 3.11 shows

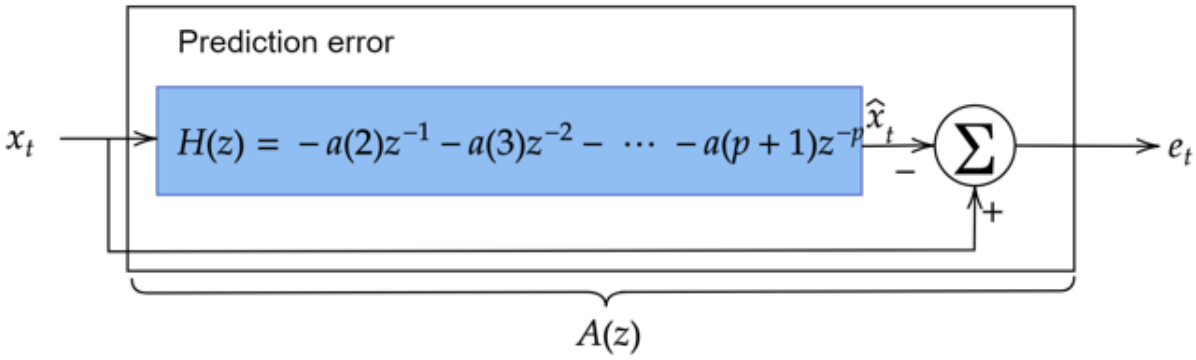

Figure 3.9: Computation of the prediction error of the AR model.

the variances based on real P-waves. According to the two figures, it can be observed that all variances are very tiny at the scale of 10^{-4} and thus, the changes in variances are not significant. That is, signals are decorrelated greatly in all cases. For instance, the prediction error variance of the Burg method decreases about 1×10^{-5} from the order of 2 to the order of 10, which is really tiny. According to two figures, the variance in the real signal case is higher than that in the simulation case. It is due to the noises and artifacts existing in the real signal. The real signal is more complicated, and the model does not fit it as well as fitting the simulate signal.

For the AR model, when p, the order increases, variances of both methods decrease, but the Burg method always has a lower variance, which means it performs better in decorrelating the input signal. It has to be mentioned that the changes are not significant, either. The variance does not change a lot after $p = 8$, meaning that increasing the order of the model can not enhance the decorrelation capability. Although the changes of variances are not significant among different orders and it can be considered that all models achieve similar decorrelating performances in two figures, combined with the results of PACF, an order no lower than 8 is good. In this case, the range of p from 8 to 12 that has been made in the last subsection is suitable. Besides, a very low order can not reflect the frequency-shaping property of the model, which will be discussed in Section. 3.6.1. Since differences of variances among different orders are not distinct, a further comparison will be made and the final order will be determined in Chapter. 5.3.

Although all ARMA models have lower variances compared to AR models, the Burg method is approximately the same. Since the scale of the variance is really tiny, i.e., the changes are not significant, the differences among different models can be omitted. The ARMA model was expected to behave better correlation removal than the AR model, i.e., much lower variance than the AR model. However, the experiments imply these two models actually have similar performance. In this case, there is no need to use the ARMA model because the AR model is computationally faster. Among the two methods of AR models, the Burg method still has a lower variance compared to the Yule-Walker method, though the difference is really small. In this case, the AR model based on the Burg method with the range of order from 8 to 12 can be used for

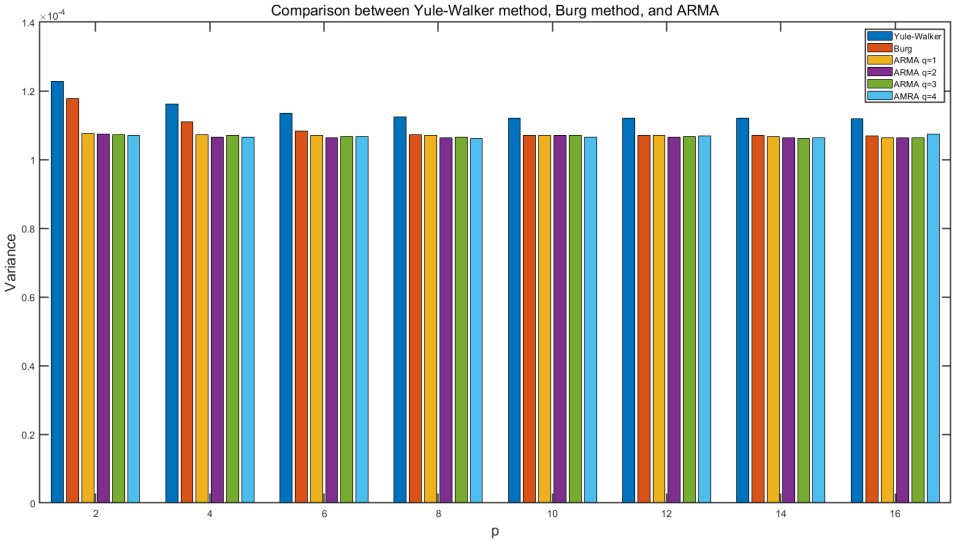

Figure 3.10: Comparison about the prediction error variance among models. The input signal is a simulated signal.

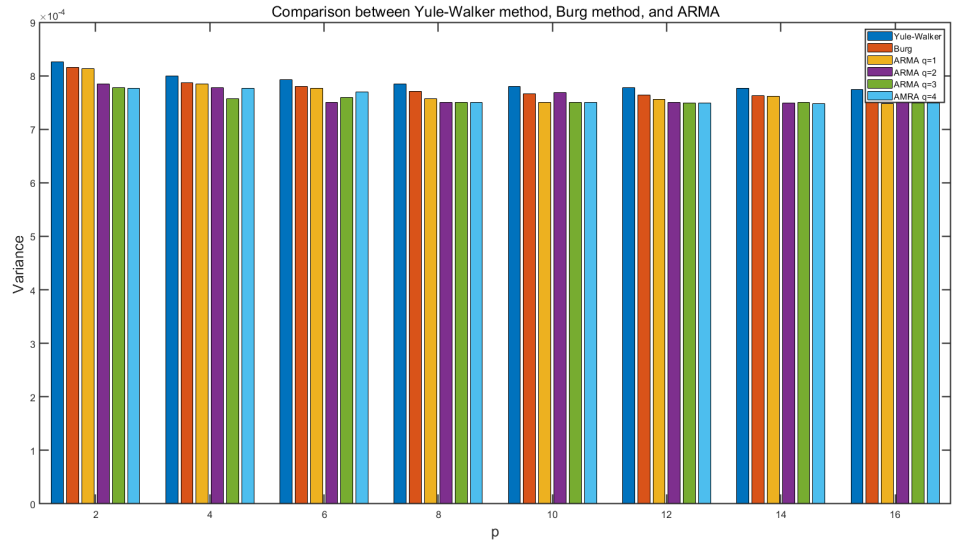

Figure 3.11: Comparison about the prediction error variance among models. The input signal is one real signal.

further experiments. It has to be mentioned that the order of the model is still not decided regarding the tiny difference in residual variances. In this case, three orders will be used throughout the following chapters. The reason for keeping using them all is that the order will impose an influence on the frequency responses of models and the information obtained, which will be discussed in the following chapters. The final order will be decided in the procedure of classification in the Chapter. 5.3.

3.6 Model Implementation

After P-wave signal is extracted by the methodology discussed in Chapter. 3.1.2 and the AR models with orders ranging from 8 to 12 based on the Burg method are decided as the models to represent the atrium, the signal can be input to models. In this section, the temporal and frequency results of signals after modeling will be given. They are related to three types of data, the simulated SR signal, the real signal in the SR scenario, and the real signal in the AF scenario. In every scenario, the ECG signal is firstly resampled to 250 Hz and filtered to remove noises. Next, the first 200 beats of the P-wave/f-wave signal are extracted as the methodology mentioned in Section. 3.1.2. Then, they are divided into 10 equal-length windows, each containing around 20 beats, as described in Section. 3.2. Although the AWL and MWL methods have different results from the quantitative perspective in the AF scenario, they can be considered the same in the idea of qualitative analysis, i.e., models based on these two methods perform the same trend on the resulting signals. Hence, considering there are too many figures to show all results of the two window methods, only the results of the MWL method will be listed. Before input, the signal is centered by subtracting the mean value.

3.6.1 Model Implementation on Simulated Signals

The simulated SR signal is produced by a well-known simulator called ECGSYN [58]. It is open-source, whose codes are provided on [38]. This simulator can generate realistic ECG waves by solving ordinary differential equations (ODE) [59]. The sampling frequency is set to 250 Hz. The mean heart rate is 60 bpm. The standard deviation of heart rate is 1 bpm. The LF/HF ratio is 0.5.

An example of the input signal and the output signal is shown in Fig. 3.12. Since there are 10 windows, it is not possible to list plots of all windows. In this case, only a few beats are shown. Besides, for the simulated signal, the AR model does not make any differences in the waveform when $p = 8$, $p = 10$, and $p = 12$. Thus, only the output signal in the AR model with the order of 8 is placed here. According to the figure, there are some discontinuities at the edges of P-waves. This is because the onset and end of P-waves in the raw ECG signal are negative values. Moreover, these discontinuities influence the resulting signal which has two impulses at the corresponding edges.

Since the AR model decorrelates the signal, one way to visualize the decorrelation is to depict the frequency spectrum. Fig. 3.13 shows an example, which is from the same window of Fig. 3.12. It is the PSD of the output signal. Same as the waveform case, the change of order does not lead to different PSDs of the output signal, and hence only the PSD of $p = 8$ is shown. This figure shows the spectrum is flat and has a value at every frequency. The autocorrelation function of the input signal and the output signal of all AR model orders is shown in Fig. 3.14. It can be observed the input signal is highly correlated and the output signal only has a high value at the lag of 0, which implies the correlation of the input signal is highly removed. The order of the AR model influences the autocorrelation of the output signal. When the order increases, the values between

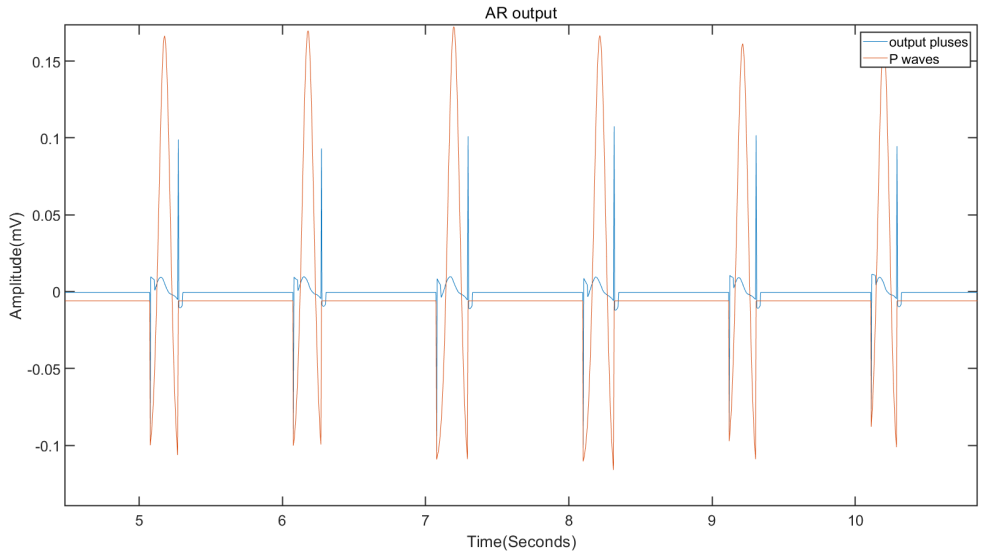

Figure 3.12: The output signal of the AR model with $p = 8$ and the input P-waves in the simulation case.

two positive peaks become lower, as marked by red blocks, meaning that the correlation is removed further. Moreover, a periodical decay pattern exists in these functions due to the repeating pulses in the time domain. In addition, autocorrelation functions in the three cases are similar, which match the similar correlation removal in the three values of p.

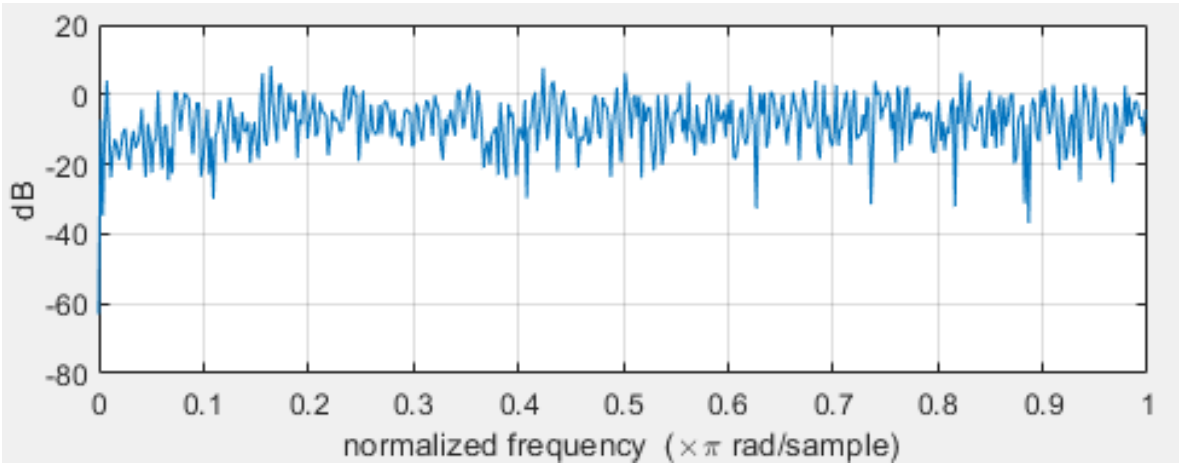

Figure 3.13: An example of the PSD of the output signal when the order of AR model is 8. It is the same window as Fig. 3.12

According to the PSD and autocorrelation function, it can be concluded that the output signal is almost decorrelated, which also verifies the low prediction error variance in Section. 3.5.2. In this case, the output signal can be considered a decorrelated pulse train, though the pulse train is not perfect. This is reasonable since the atrium is not

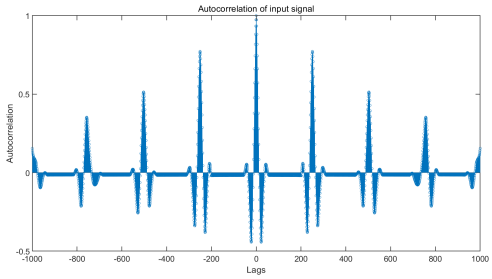

(a) Input signal

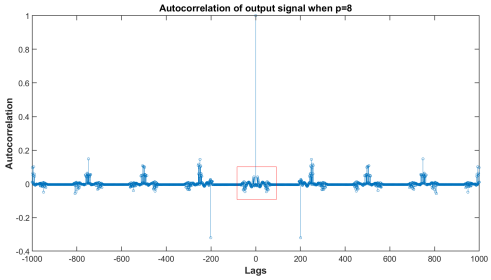

(b) p=8

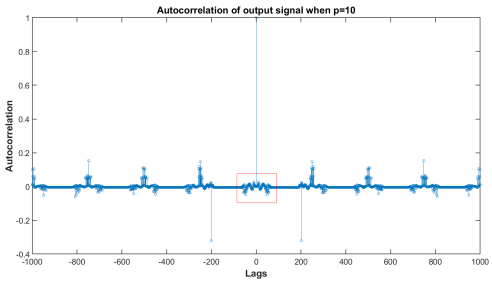

(c) p=10

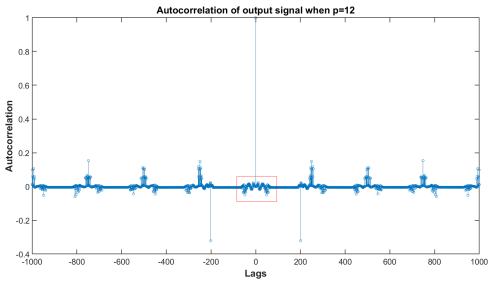

(d) p=12

Figure 3.14: The autocorrelation of the input signal and the output signal after processing by the AR model with different orders. It can be observed the correlation is highly removed by comparing (a) and (b-d). For a pulse train, the autocorrelation is periodically decayed in (b-d).

an AR model in nature. The idea mentioned in Chapter. 2.5 is validated by the results.

The frequency responses of the AR model are depicted in Fig. 3.15 and Fig. 3.16. The former gives a response of the AR model with different orders on one window of the signal, which is from the same 3rd window. According to the figure, one peak is observed, which implies the characterization of the atrium made on the pulse train sent by the SA node. This kind of peak in the speech signal is called 'formant', functioning the voiced pitch that is also an impulse train into a speech signal. In a similar manner of thinking, it can be considered that the atrium models the pulse train into P waves by shaping the frequency spectrum and concentrating the signal energy at the formant frequency. In addition, it can be discovered that the increasing order shapes the frequency peak sharper. This results from more coefficients being used to model the atrium.

Frequency responses of all windows are shown in Fig. 3.16 by stacking responses together. Only $p = 8$ is listed here since the differences are not prominent among orders ranging from 8 to 12 in the simulation case. Although Fig. 3.10 and Fig. 3.11 show that the order 2 or 4 is sufficient for the prediction error variance, the frequency responses, which are shown in Fig. 3.17 and Fig. 3.18, can not perform a formant in these two cases. In this case, it can be understood that the order should be appropriately high to model the formant of P-waves. Each line in Fig. 3.16 represents the response of a window in the figure. Every window has the same response because the signal is simulated and has no artifacts or disturbances. By using the simulated signal, the

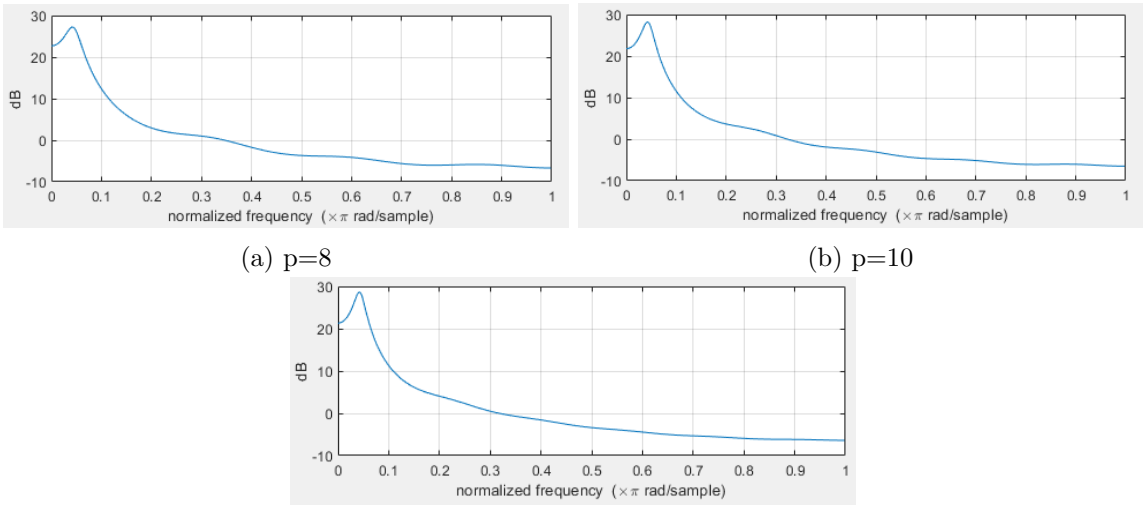

(a) p=8 (b) p=10

(c) p=12

Figure 3.15: The frequency response of the AR model implemented on the same window as Fig. 3.12.

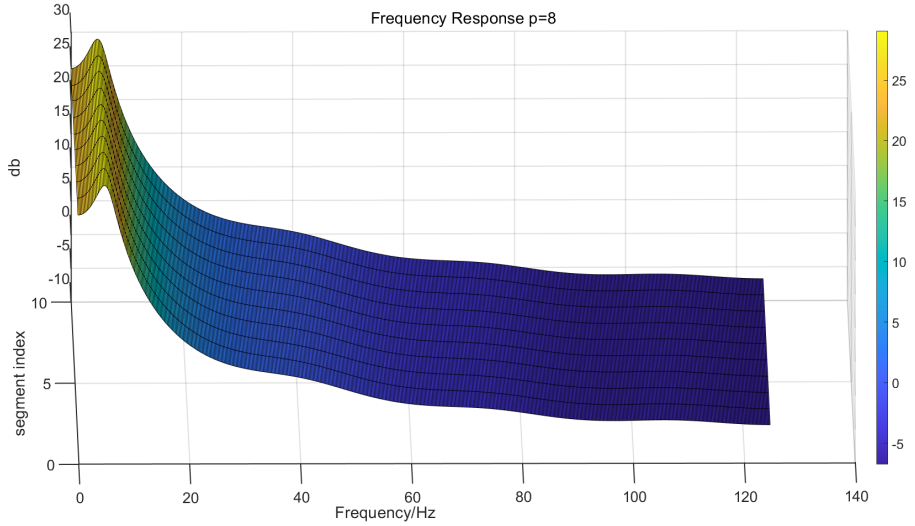

Figure 3.16: The frequency responses of the AR model implemented on all windows when $p = 8$ when the input of the model is a simulated signal.

AR model can give some reference results which are beneficial when implementing the model on a real dataset. Results from the real signals will be discussed in the next section.

3.6.2 Model Implementation on SR Signals

In this section, the real SR signals are used, where the conditions are more complex compared to the simulation case. The dataset used is MIT-BIH normal sinus rhythm

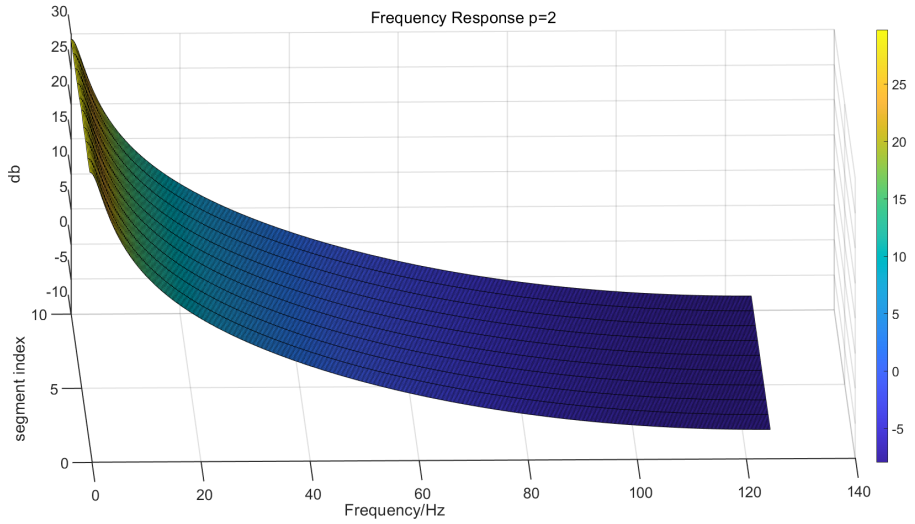

Figure 3.17: The frequency responses of the AR model implemented on all windows when $p = 2$. Although the prediction error variance is small, the formant is not modeled.

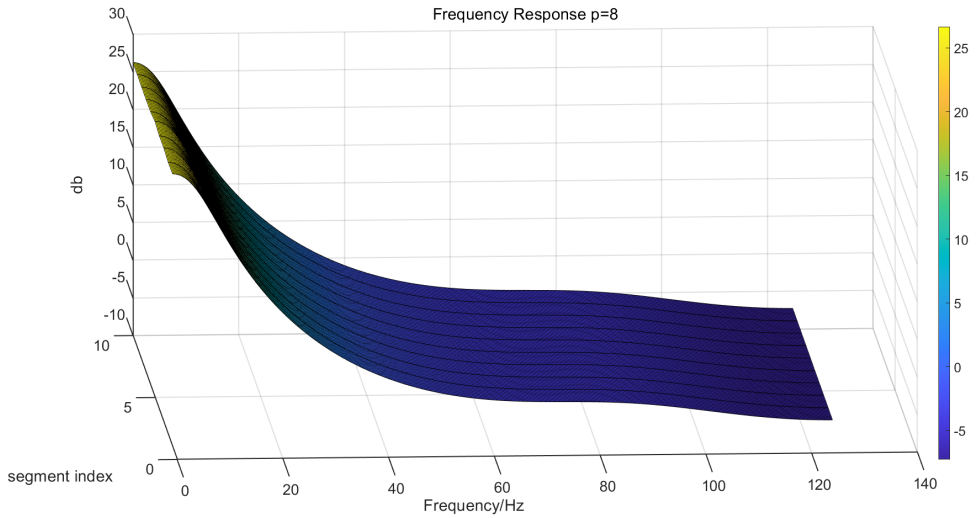

Figure 3.18: The frequency responses of the AR model implemented on all windows when $p = 4$. Similar to $p = 2$, the formant of P-waves is not modeled.

database which is a public dataset [38]. This dataset consists of 18 long-term SR ECG recordings with two leads. Since the AR model only requires a single signal, recordings from the first lead are used. Considering that there are too many plots for all recordings, only results related to one recording are listed as examples in this section. The overall methodology is the same as the simulated signal.

The input and output signals in several beats are plotted in Fig. 3.19 as an example. The amplitude of P-waves is multiplied by 2 such that both signals can be observed obviously and there is no overlapping in the figure. Since the order of the AR model does not have a large influence on the waveform, only the $p = 8$ case is listed. In

addition, the amplitude of P-waves is scaled by 2 in order to show clearly. The figure shows that if the input signal is contaminated by noises, the model will also model some noises. The PSD of the output signal when $p = 8$ is depicted in Fig. 3.20, which shows the output signal is decorrelated with a white spectrum. Only the $p = 8$ case is listed since various orders of the AR model do not cause a large difference in the PSD of the output signal.

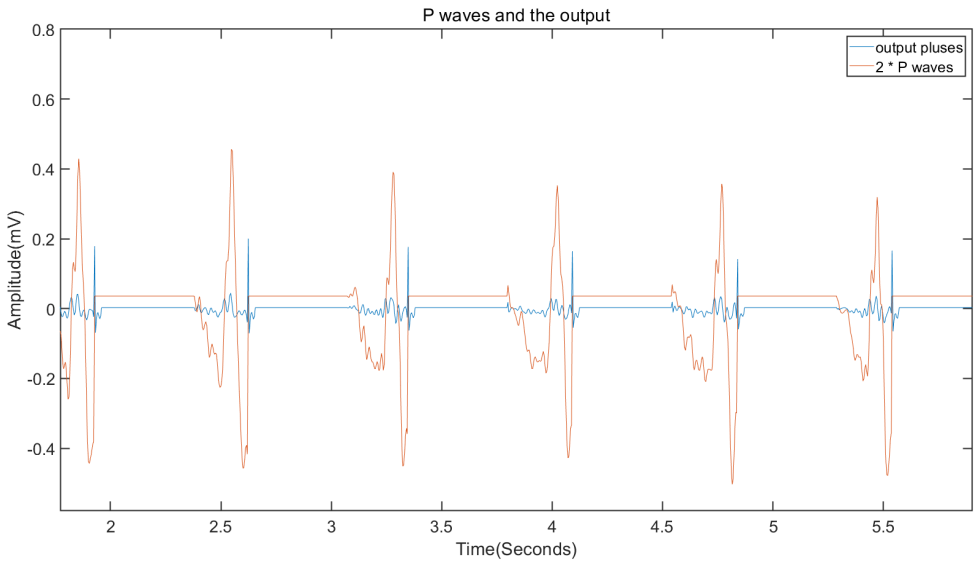

Figure 3.19: The output signal of the AR model with $p = 8$ and the input P-waves in the real signal case. To better compare two signals, the amplitude of the P-waves is multiplied by two. Otherwise, there is an overlapping of waveforms in the figure.

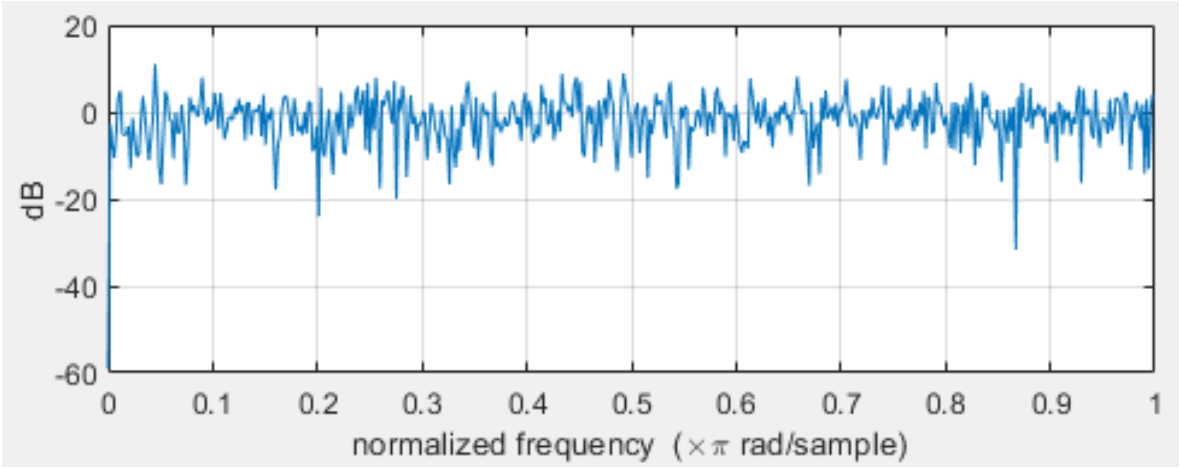

Figure 3.20: An example of the PSD of the output signal when the order of AR model is 8 in the real SR signal case.

The autocorrelation function of the input signal and the output signal is given in Fig. 3.21. Similar to the situation when the input is a simulated signal, the correlation is

highly removed. In addition, the residual correlation in the red blocks decreases when the order increases. Moreover, the smallest negative value between $Lag = 0$ and the second peak is not as prominent as the simulation case. It can be concluded from Fig. 3.20 and Fig. 3.21 that the input P-waves are decorrelated by the AR model. Hence, the idea in Chapter. 2.5 is validated by the real data.

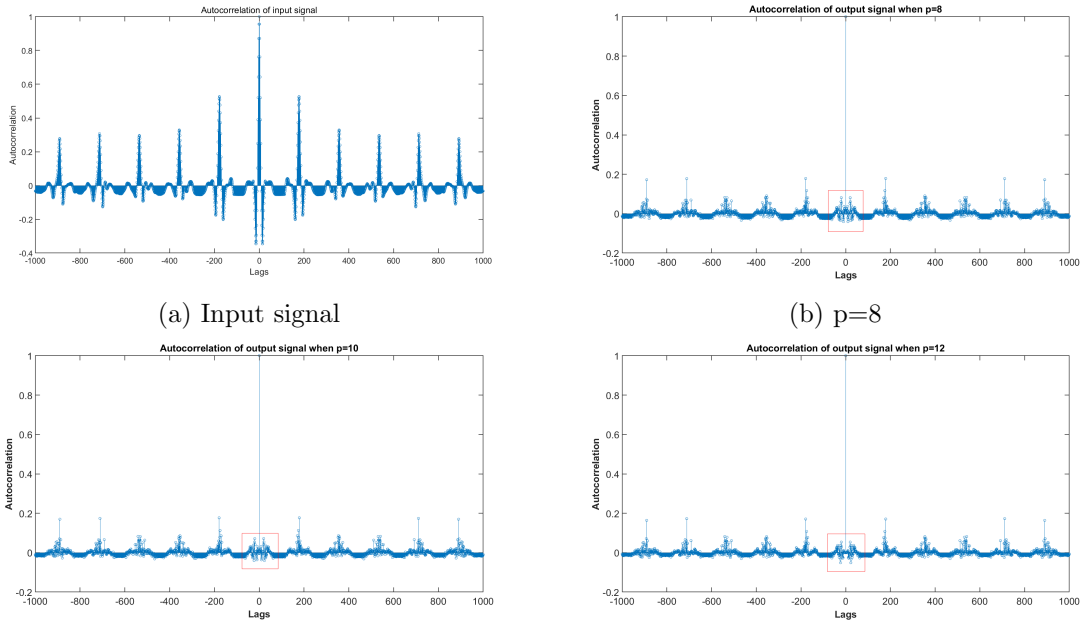

(a) Input signal

(b) p=8

(c) p=10

(d) p=12

Figure 3.21: The autocorrelation of the input signal and the output signal after processing by the AR model with different orders in the real SR case. It can be observed that the correlation is removed by comparing (a) and (b-d).

The frequency responses of a single window in the AR model with different orders are shown in Fig. 3.22. Three figures come from the same window. Through (a), (b), (c), it can be observed that increasing p contributes to concentrating the energy of the waves, which is similar to the simulation scenario. Besides, as the order increases, another peak appears gradually at the normalized frequency of around 0.25. This peak does not reflect the P-waves, instead. The first reason is that the frequency band of P-waves does not reach such a high frequency which is 31.25 Hz. Fig. 2.5 suggests the frequency band of the whole ECG signal is lower than 30 Hz. [22] also mentions P-waves is normally considered below $10 - 15$ Hz. The second reason is that PSD of the simulated case only shows one formant when the order is 12. Hence, the other emerged peak implies that some coefficients of the model are allocated to the noise representation, and the spectrum and energy of noises are modeled. Fig. 3.23 shows the stack of responses of all windows. When $p = 12$, another peak starts to appear at around 30 Hz, which is in accordance with Fig. 3.22.

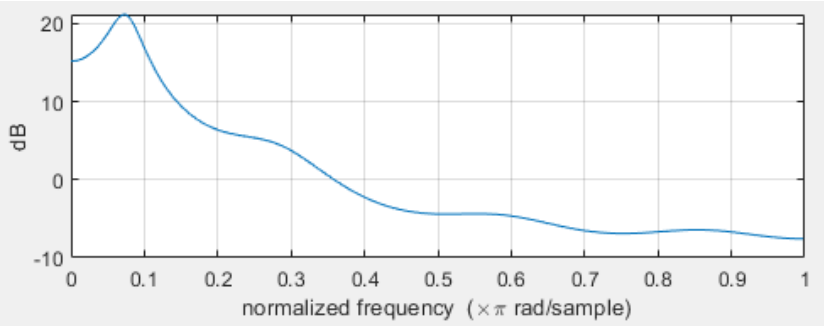

(a) p=8

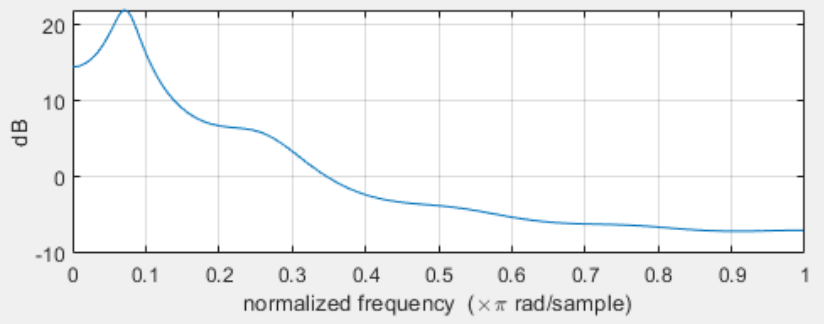

(b) p=10

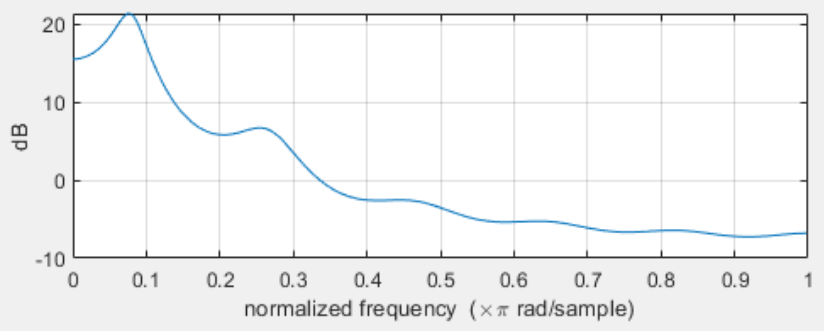

(c) p=12

Figure 3.22: The frequency response of the AR model with different windows implemented in a single window. The input signal is the SR signal.

These results, based on the simulated signal and the real SR signal, provide an interpretation of the AR model modeling the atrium. It gives information related to the single formant and implies the way of shaping P-waves. In this case, the AR model can be considered a pulse-shaping filter, and thus, the atrium is discovered as a pulse-shaping filter. The input electrophysiological pulse train sent from the SA node is modeled by the atrium as the series of P-waves in the way that the atrium shapes the frequency spectrum of the pulse train.

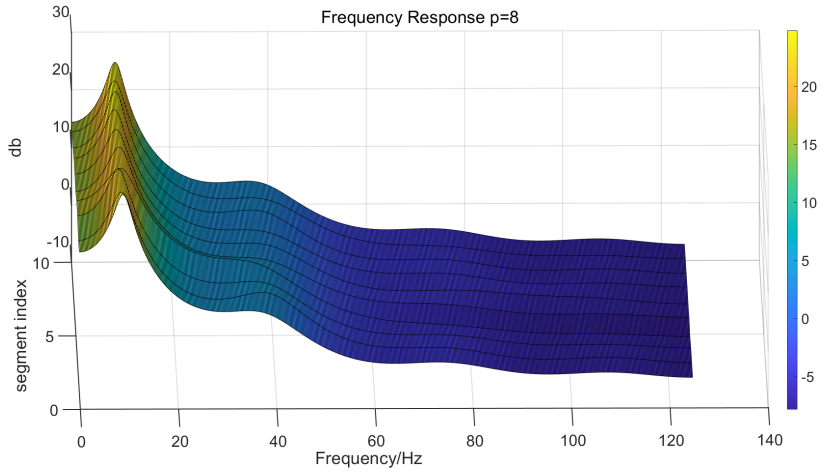

(a) p=8

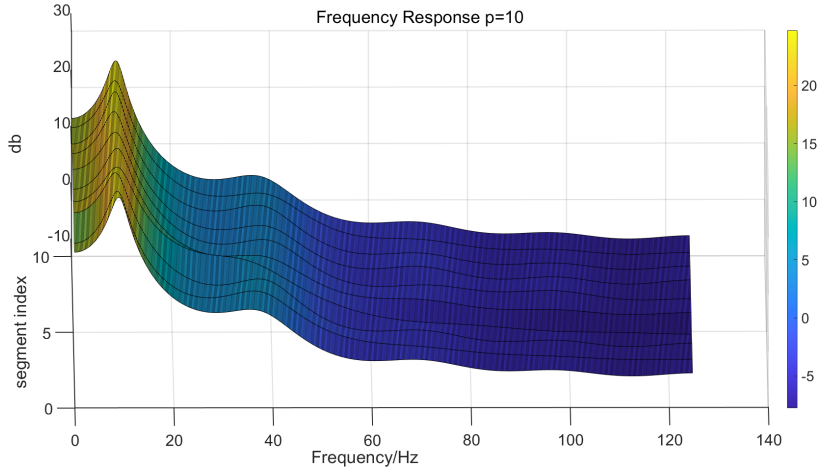

(b) p=10

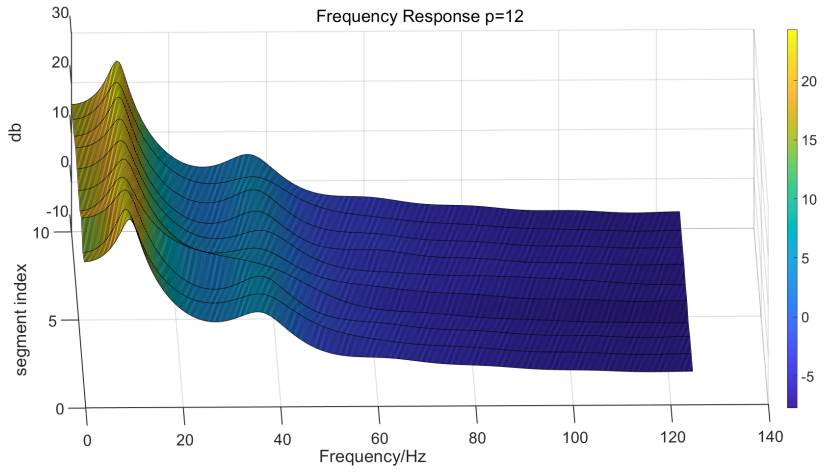

(c) p=12

Figure 3.23: The frequency responses of the AR model with different orders implemented on all windows. The input signal is the SR signal.

The reason for the existence of these formants is that P-waves are not simple, single-frequency signals, although their waveforms look like they are sinusoidal. Many myocardial cells contribute to the formation of a P-wave through depolarization. This is because the electrical wavefront propagating through the atrium activates these cells in different regions at slightly different times. Since P-waves are the summation of electrical activities of all atrial myocardial cells, these different temporal activations lead to the composite frequency of P-waves. Hence, multiple frequency components exist in P-waves, which have different frequency bands and different energies. Therefore, there becomes a formant that gathers the most energy of those different frequencies. Besides, only a single formant exists in a signal segment due to the coordinated activation and conduction of atrial myocardial cells. The wave propagates quickly and uniformly through these cells and causes coordinated activation, leading the single formant to emerge.

3.6.3 Model Implementation on AF Signals

Since AF is a common but risky disease and detection of it is one of the goals of this thesis, the AF signals are used in order to evaluate how the parameters change. In this section, the real AF signals are used, where the results can be expected to be very different. The dataset used is the MIT-BIH atrial fibrillation database which is also a public dataset from the physionet website [38, 60]. Twenty-three recordings from AF patients are included in the dataset, most of whom are paroxysmal AF patients. The dataset also contains two leads recordings and the first one is implemented. The onset and end of AF segments are annotated in the dataset and used to extract pure AF signals for experiments. Only the recordings which have more than 200 beats AF are used because the AR model requires the input signal to have 200 beats in total. In addition, since the overall model in this thesis should be universal for all kinds of ECG signals, whether AF or SR, the same methodology as the other two scenarios are implemented. However, one thing has to be mentioned is that the extraction method mentioned in Chapter. 3.1.2 only extracts the part of AF components that exist between QRST complexes. Since there are too many recordings and will be too many figures if the results of all recordings are shown, only the results of one recording are listed as examples.

Fig. 3.24 shows the waveforms of the output signal and f-waves. In the AF case, it can be observed the input process becomes chaotic and irregular compared to the SR case, which causes the chaotic performance on the output signal. The output frequency is shown in Fig. 3.25, inferring that the output signal has a white spectrum and hence is decorrelated. Since the PSD is similar for the AR model with different orders, only the $p = 8$ case is listed here.

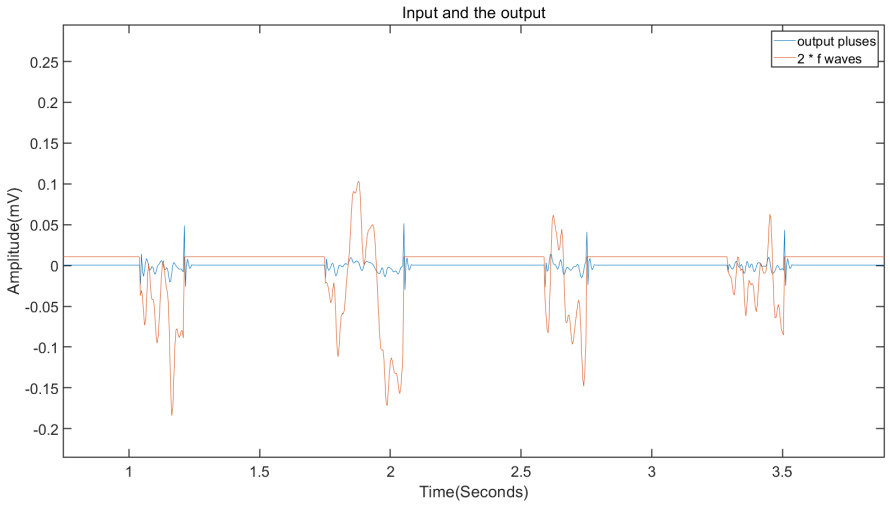

Figure 3.24: The output signal of the AR model with $p = 8$ and the input P-waves in the AF case. The amplitude of the P-waves is multiplied by two such that the waveforms of two signals can be observed obviously. Otherwise, there will be an overlapping of two waveforms in the figure.

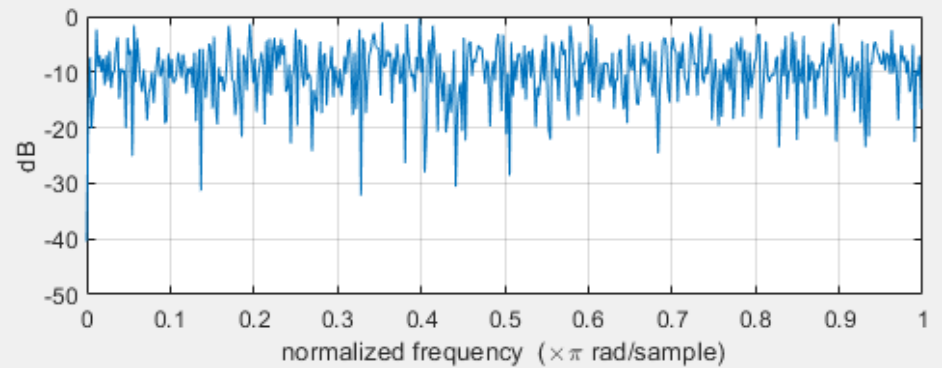

Figure 3.25: An example of the PSD of the output signal when the order of AR model is 8 in the AF case.

Besides, the autocorrelation of the input signal and the output signal is revealed in Fig. 3.26. Comparing (a) and (b-d), it can be observed that the correlation is removed, like the simulation and SR cases. Similar to the autocorrelation function in the SR case, the increasing order leads to lower values of autocorrelation encircled in the red blocks. The difference is that these functions become more chaotic and complex than them in the SR case. To be specific, the figure does not show the naive pattern of the autocorrelation function, which contains a high value of 1 at lag 0 and performs periodical decay due to the repeating pulses in the time domain.

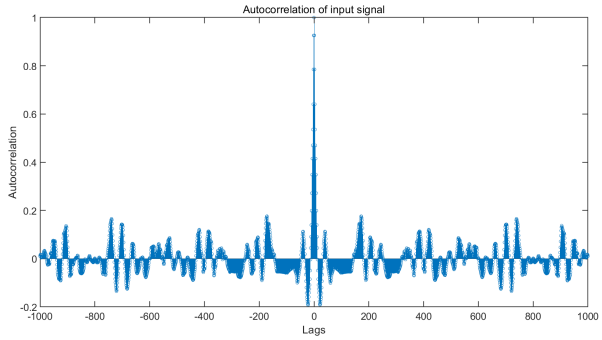

(a) Input signal

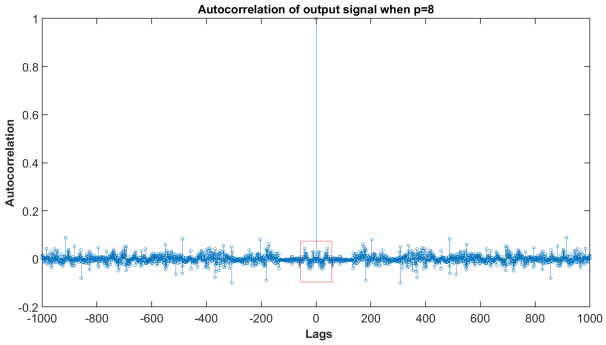

(b) p=8

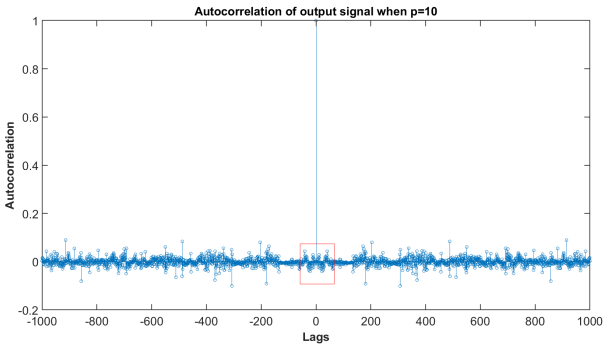

(c) p=10

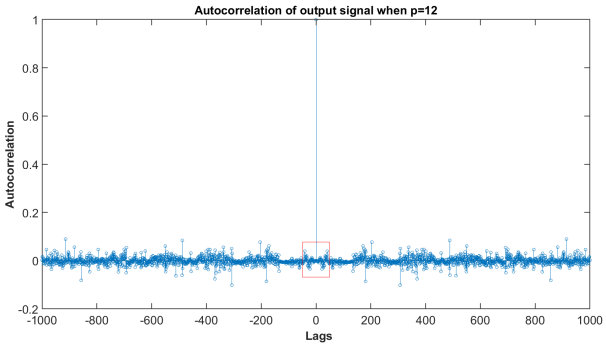

(d) p=12

Figure 3.26: The autocorrelation of the input signal and the output signal after processing by the AR model with different orders. The input signal is the AF signal. Similar to former cases, the correlation is removed. The autocorrelation in (b-d) becomes chaotic compared to the SR case.

The responses of the AR model of one window and all windows are plotted in Fig. 3.27 and Fig. 3.28. It can be observed in Fig. 3.27 that AF arises a different pattern of the filter's frequency response compared to the SR case or the simulation scenario. The peak disappears and the energy is distributed when $p = 8$ and $p = 10$. A potential peak arises when the order increases to 12 because too many AR coefficients are used to model f-waves plus artifacts. In this case, the model can be considered overfitting instead of fitting well. In addition, not all windows have this kind of peaks, as shown in Fig. 3.28. This also implies the model is overfitting in the first several windows. Otherwise, the peak pattern should appear in all windows.

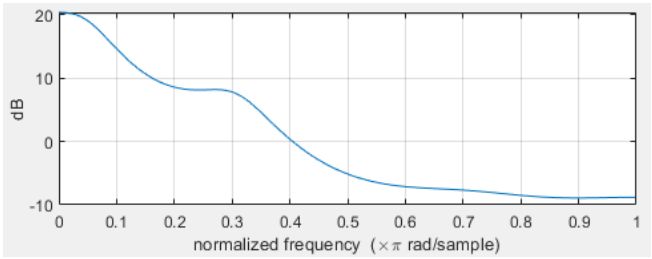

(a) p=8

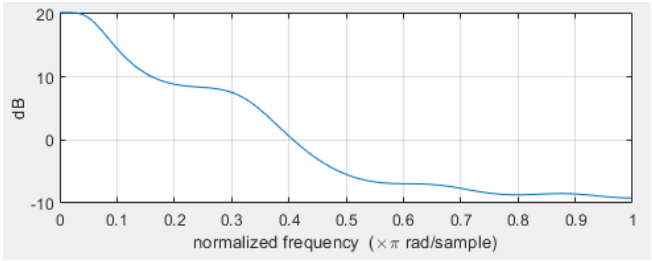

(b) p=10

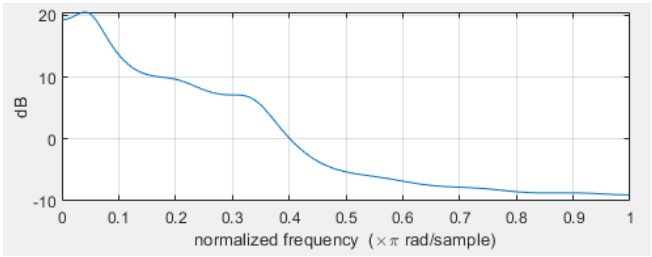

(c) p=12

Figure 3.27: The frequency response of the AR model with different windows implemented in a single window. The input signal is the AF signal.

The disappearance of the formant implies that the myocardial cells are not activated in the coordinated fashion as in the SR case. In a heart suffering from AF, the pathological changes make it difficult for electrical waves to propagate uniformly and follow the one-way direction. The normal electrical pathways may get blocked, and the waves may propagate through some abnormal pathways. In this case, myocardial cells are not activated coordinatedly and even initial activities spontaneously, contributing to the chaotic frequency components resulting in the chaotic frequency response.

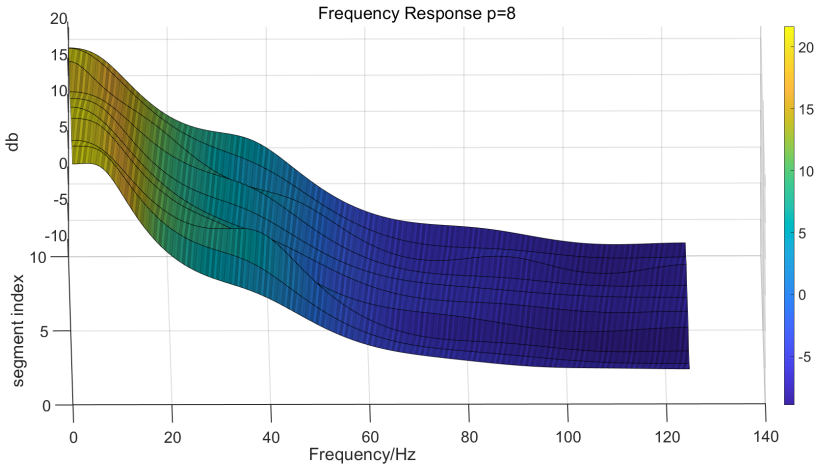

(a) p=8

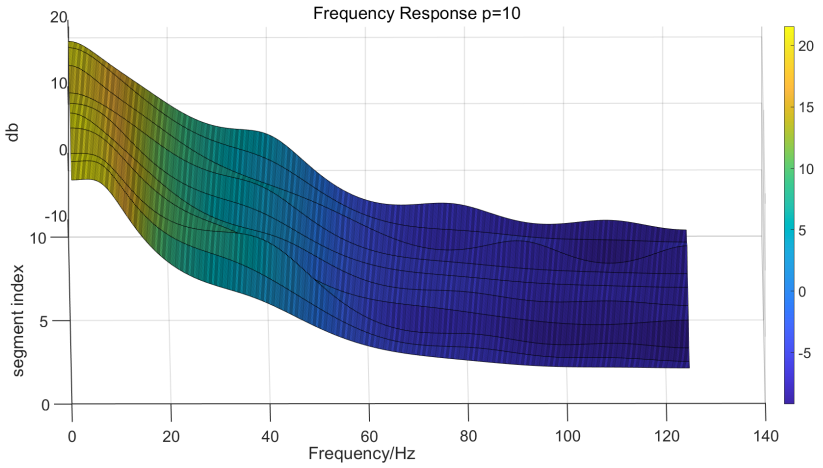

(b) p=10

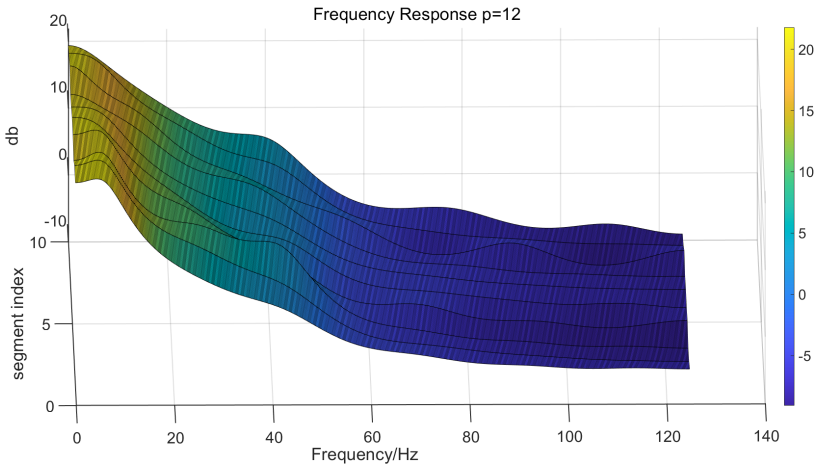

(c) p=12

Figure 3.28: The frequency responses of the AR model with different orders implemented on all windows. The input signal is the AF signal.

3.7 Chapter Summary

This chapter mainly focuses on proposing the atrial model based on the idea of Chapter. 2.5. The noises are firstly reduced and P-waves are extracted. These two steps compose the pre-processing of this thesis, as highlighted in Fig. 1.1. Then, the signal stationarity is assessed to fulfill the pre-requisition of models. The AR models and ARMA models are evaluated and the AR model based on the Burg method is considered as the final model, whereas the order is not determined and varies from 8 to 12. According to the results in this chapter, the single formant of P-waves is modeled. It is a representation that the atrium activities generate the P-waves by shaping the frequency spectrum of the input pulse train. The potential connection between the formant and the physiological information of the heart is built. The order of the model influences the frequency response of the model because a higher order means more coefficients are used to model the signal components regardless of P-waves or noises. In this case, the order will also influence the information obtained from the parameters, which will be discussed in the next chapter.

Interpreting Information from AR models

4

After obtaining the model parameters and results of signals, the interpretation can be completed. This chapter will discuss two perspectives of interpreting information from AR models, corresponding to the interpretation block in Fig. 1.1. The zero-pole plot will first be used in Section. 4.1, where the locations of poles reflect the modeling of P-waves. Moreover, formants will be estimated in Section. 4.2. Finally, the ECG modeling will be done and compared to the P-waves modeling in Section. 4.3, conveying that the whole ECG signal is not applicable in the model.

4.1 Zero-pole Plot

As discussed in Chapter. 3, the frequency responses of the AR model in the SR case and the AF case are different due to the extraction of different waves. Although the filter composed by these AR coefficients reflects the resonance frequency and formant, these coefficients are only some numbers and need to be interpreted in a more informative manner. One way to achieve this is to use the zero-pole plot which is a graphical representation of the system function. An advantage of this representation is that it maps the one-dimensional model parameters into the 2-dimensional space such that it is easier for clustering.

By observing Eq. 2.8, it is understood that the AR model is an all-pole model. Therefore, there are some poles with one zero point at the origin. Locations of these poles are derived by solving the roots of the polynomial in the denominator of Eq. 2.8,

$$H(z) = \frac{1}{A(z)} = \frac{1}{\prod_{i=1}^{p}(1 - s_i z^{-1})} \tag{4.1}$$

where s_i is a complex number. Among these poles, there is always a pair of conjugate complex numbers. Hence, the locations of these poles are symmetric in principle. In addition, all poles lie within the unit circle since the AR model is invertible.

As described before, since the number of figures of results from all recordings is large, only two examples of SR and AF results are shown. The recordings are the same as SR and AF recordings used in Chapter 3.

The zero-pole plots of the AR model based on the SR recording are depicted in Fig. 4.1. The figure shows that as the order of the AR model increases, the number of poles also increases. Since these poles are arranged regularly, they can be considered clusters. For instance, when $p = 8$, there are eight clusters of poles. Moreover, compared to the situation of a lower order, most poles in a higher order, like $p = 12$, become distributed chaotically, which means the increasing order leads modeling of noises and

artifacts. Nevertheless, there is a cluster that hardly changes, which is the first cluster going counterclockwise along the x-axis. It becomes more concentrated as the order increases. This cluster actually represents the most energy of the frequency of P-waves, which are the peaks in the frequency response of Fig. 3.23. This cluster is desired since it represents the resonance information of the atrium. In (a), a red circle is used as an example to mark the cluster of poles representing the frequency of P-waves.

The zero-pole results based on the AF signal are shown in Fig. 4.2. It can be observed that all poles spread chaotically and not as concentrated as in the SR case. It implies the energy dispersion in the spectrum of the F-waves. This is due to the dysfunction of the atrium, i.e., the atrium does not have the capability of shaping the receiving impulse as a kind of wave with a particular resonance frequency. Besides, the figure shows that when $p = 8$, the poles other than these desired poles can still be considered to form clusters. These dispersed poles tell that when AF happens, the atrium losses the capability of generating normal waves.

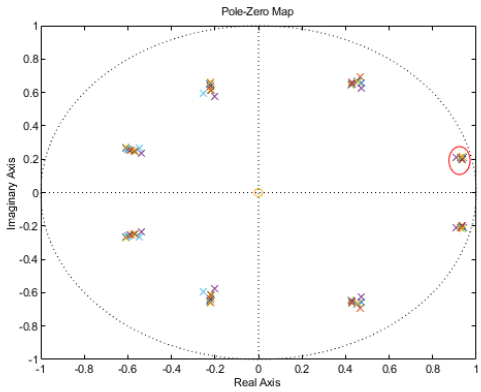

(a) p=8

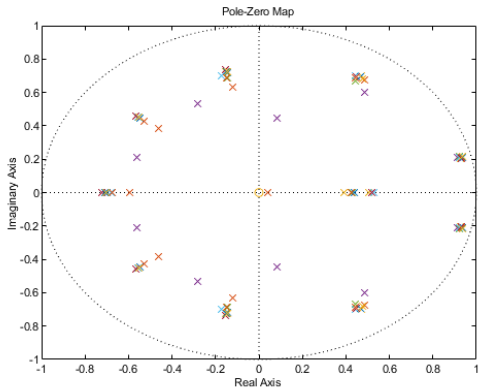

(b) p=10

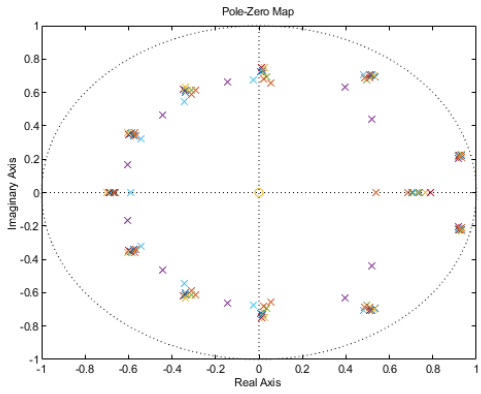

(c) p=12

Figure 4.1: The zero-pole plots of the AR model based on the SR recording. The red circle in (a) marks the desired cluster of poles.

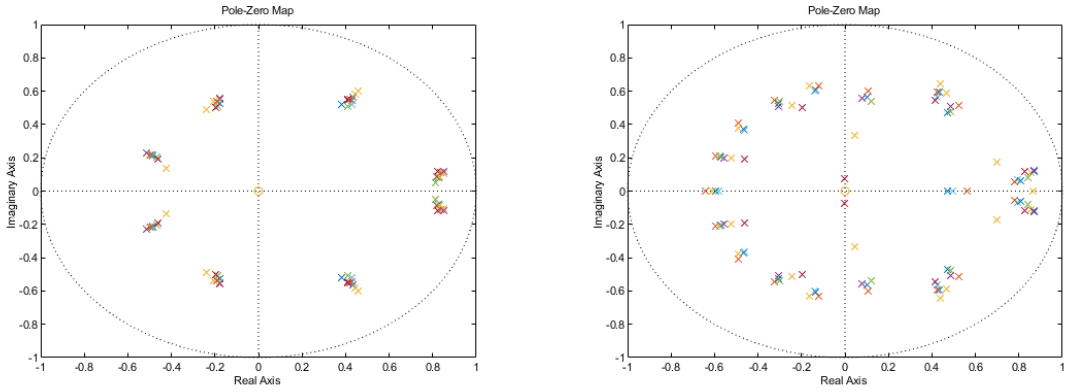

(a) p=8 (b) p=10

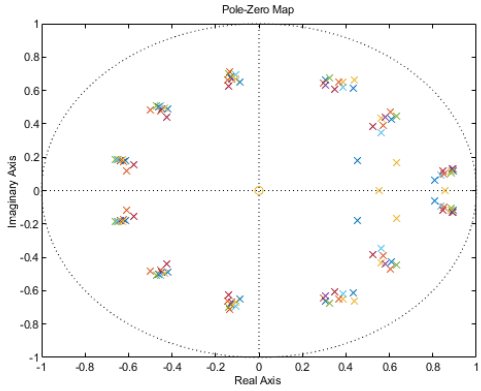

(c) p=12

Figure 4.2: The zero-pole plots of the AR model based on the AF recording. The poles of the model are more dispersed than those of the SR case.

4.2 Poles and Formants

4.2.1 Formants Estimation

Zero-pole plots have been achieved in the last section. To better interpret the frequency of the poles, the formant estimation is implemented. The locations of roots calculated from the polynomials of the AR model represent the information of formants. The frequencies of formants in the angular form are estimated by

$$\Omega_i = atan2(Im(s_i), real(s_i)) \tag{4.2}$$

where $atan2()$ measuring the angle between the x-axis and the ray from the origin to the root s_i is given by

$$atan2(x,y) = \begin{cases} arctan\left(\frac{y}{x}\right), & x > 0 \\ arctan\left(\frac{y}{x}\right) + \pi, & y \geq 0, x < 0 \\ arctan\left(\frac{y}{x}\right) - \pi, & y < 0, x < 0 \\ +\frac{\pi}{2}, & y > 0, x = 0 \\ -\frac{\pi}{2}, & y < 0, x = 0 \\ 0, & y = 0, x = 0 \end{cases} \tag{4.3}$$

It has been shown in Chapter. 3.6.1 and Chapter. 3.6.2 that there is only a single formant in the spectrum of the P-waves. When the order of the AR model increases, the simulation results show no new formant emerges, and the real SR signal shows the newly appeared formant is located at around 31.25 Hz and thus corresponds to the noises. Hence, it can be considered that P-waves only contain one formant.

Since these roots always appear in pairs, only the roots whose imaginary part is positive are included. Afterward, the angular frequencies can be converted into frequencies in Hz. Considering the desired pole is the first pole with a non-zero imaginary part and there is a single formant, the frequency of it is the smallest positive value among all estimated frequencies. Although only the AR model implemented on SR signals can perform formants in the frequency response, the same methodology is done on the AR model based on the AF signals since the overall model should be general. The estimated frequencies $\hat{f}$of the example SR recording and AF recording are listed in the table below.

Window Index	$\hat{f}$ when $p = 8$ (Hz)	$\hat{f}$ when $p = 10$ (Hz)	$\hat{f}$ when $p = 12$ (Hz)
1	8.94	9.01	9.44
2	8.88	8.81	8.96
3	8.37	8.57	9.28
4	9.14	9.01	8.77
5	8.95	9.07	9.58
6	8.56	8.82	9.32
7	8.37	8.58	9.37
8	8.68	8.78	9.29
9	8.73	8.84	9.19
10	8.99	9.05	9.56

Table 4.1: The estimated formant frequencies of the example SR recording with different orders of the AR model.

According to these two tables, it can be observed that the AR filter based on the SR signal models a more concentrated set of formant frequencies than the AF signal. In other words, whilst modeling the AF signal, there is a larger variation in these frequencies which are represented by the poles standing in similar locations to the SR case. This is consistent with the zero-pole representation. The estimated zero frequency

Window Index	$\hat{f}$ when $p = 8$ (Hz)	$\hat{f}$ when $p = 10$ (Hz)	$\hat{f}$ when $p = 12$ (Hz)
1	5.01	5.25	5.28
2	5.17	5.62	5.64
3	4.90	5.05	5.19
4	5.50	5.72	5.66
5	2.33	3.77	4.62
6	4.27	3.39	4.36
7	5.50	5.51	5.56
8	3.91	2.99	2.91
9	4.25	2.79	4.69
10	4.12	9.59	0

Table 4.2: The estimated formant frequencies of the example AF recording with different orders of the AR model.

means the window lacks a pole in the certain area and has the pole on the x-axis, which leads to a tremendous variation. Moreover, it can be discovered that these estimated frequencies increase as the order increases. Hence, the order of the model also influences estimated frequencies.

4.2.2 Analysis of poles and formants

Although the frequency responses and the zero-pole plots are shown above, it is better to draw them together such that the relationship between the poles and frequency responses can be explored. In this case, the 3-d plots containing zero-poles and frequency responses with different model orders are depicted in Fig. 4.4, Fig. 4.4, and Fig. 4.5.

According to these figures, it can be observed that the shape of frequency responses is highly connected to the distribution of poles. To be specific, the first cluster of poles in (a) in Fig. 4.3 locates at the position of the peak of frequency responses, which means they determine the resonance frequency in the responses. In addition, these poles are near the unit circle that is plotted by the red dotted line. Since the distance between a pole and the origin defines the amplitude of the response at this frequency, the near-unit-circle positions contribute to the peaks of formants. However, a different situation is discovered by looking at the 3-d plots of the AF case in (b) in Fig. 4.3. When AF occurs, these desired poles move further inner the unit circle rather than close to it, generating quite flat frequency responses. Besides, these poles in the AF case move toward the real axis, meaning that the frequency represented becomes lower and no peaks appear.

Since the relationship between the coordinated activity of myocardial cells, the uniform propagation of electrical waves, and the appearance of the formant is analyzed in Chapter. 3.6, it can be inferred that the concentration of poles actually implies the degree of the coordinated activations of these cells. In the SR scenario, the electrical wave propagates uniformly and myocardial cells are activated coordinately, resulting in the concentrated poles. However, in the AF scenario, poles in the desired cluster become

greatly dispersed. This observation describes the chaotic activation of myocardial cells, which results from the chaotic wave propagation and spontaneous activations of cells.

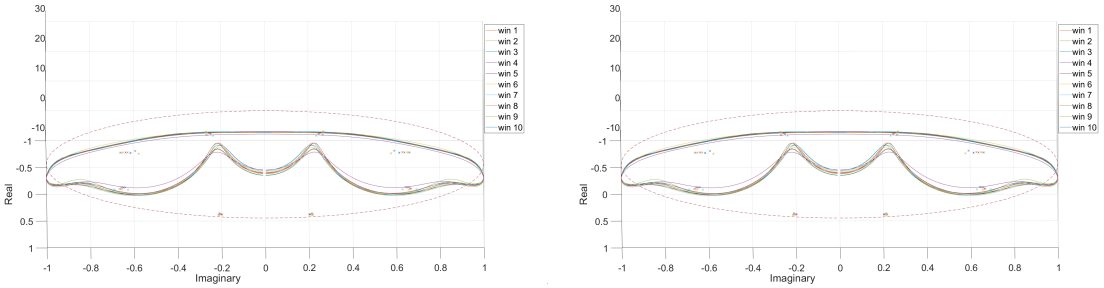

(a) The 3d plot in the SR case. (b) The 3d plot in the AF case.

Figure 4.3: The 3d plots when $p = 8$.

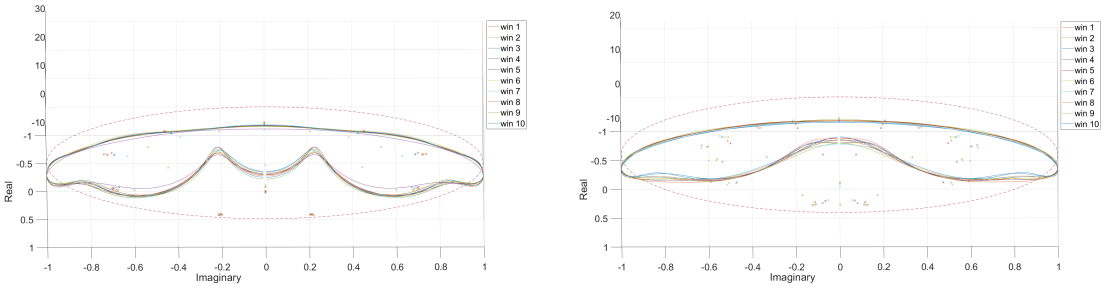

(a) The 3d plot in the SR case. (b) The 3d plot in the AF case.

Figure 4.4: The 3d plots when $p = 10$.

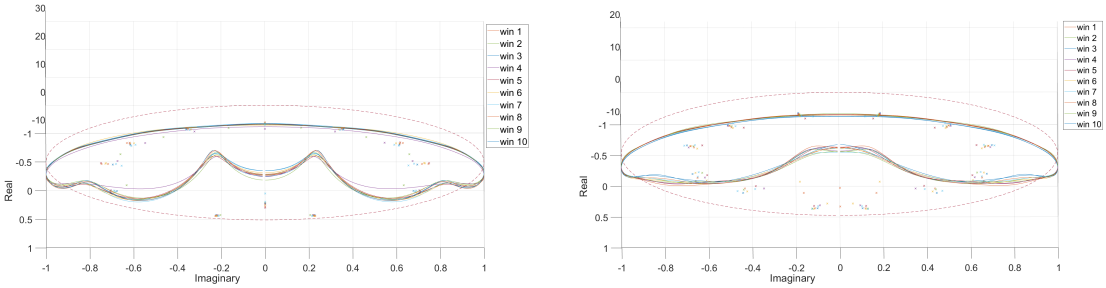

(a) The 3d plot in the SR case. (b) The 3d plot in the AF case.

Figure 4.5: The 3d plots when $p = 12$.

4.3 Comparison with the ECG Modeling

It has been introduced in Chapter. 2.4.4 that some literature exploits the combination of AR parameters and machine learning techniques to achieve the classification of SR and AF ECG signals. However, machine learning techniques, like the generalized linear model, the k-nearest neighbor, and the support vector machine [33, 34, 61], do not

exploit the information related to the physiological structure of the heart. This is why this thesis turns to model the atrium parametrically based on P-waves. However, what if the atrium can also be modeled based on the ECG signal? If the total ECG recording is applicable in the same methodology, it is potentially better to use ECG since the problem of discontinuity brought about by the P-waves extraction can be overcome. In this section, the whole ECG recording will also be implemented, and the results will be compared with those in the P-waves case. Instead of using signals from the SR recording, the SR signal and AF signal are both from the AF recording in order to evaluate the frequency change in ECG signals resulting from the atrium dysfunction.

Firstly, like the process in Chapter. 3.5.2, the order of the AR model should be determined by correlation removal. The prediction error variances from AR models with different orders are shown in Fig. 4.6 when the input signal is the SR signal. The figure shows the variances among different windows when the order changes. It can be observed that variances do not decrease after $p = 8$. Hence, the order can be considered $p = 10$. Besides, the variances of ECG signals are much larger than those of P-waves, which means residual correlations existing in the post-processed signals are larger.

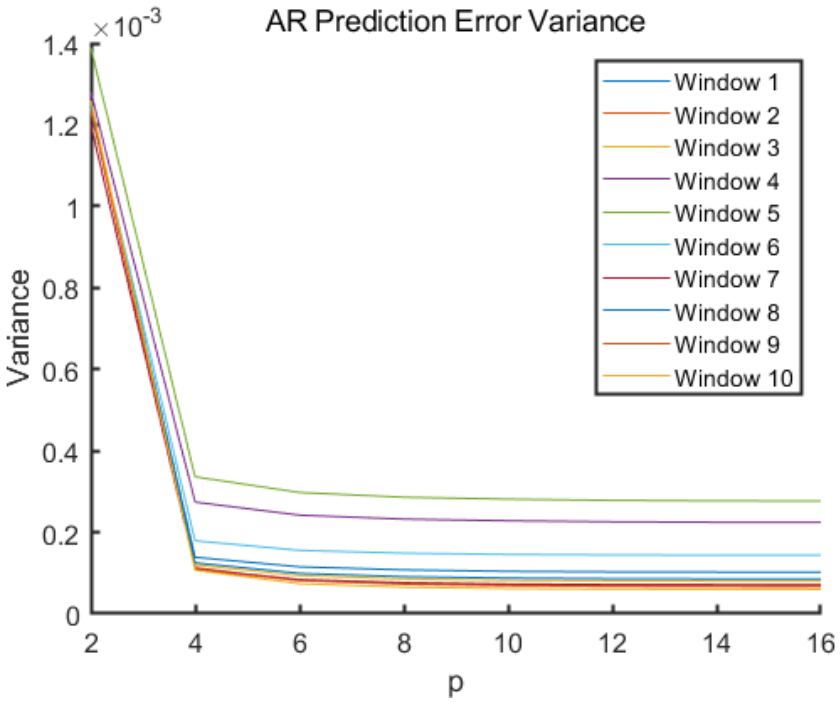

Figure 4.6: Prediction error variance of ECG signals in the SR case.

In addition, the frequency responses of all AR models based on the SR ECG and the AF ECG are depicted in Fig. 4.7. According to the figure, the responses in the two cases do not exhibit different patterns: both perform about three peaks. In this case, the responses can not convey the information related to the P-waves since the existence of P-waves does not influence the morphology of responses.

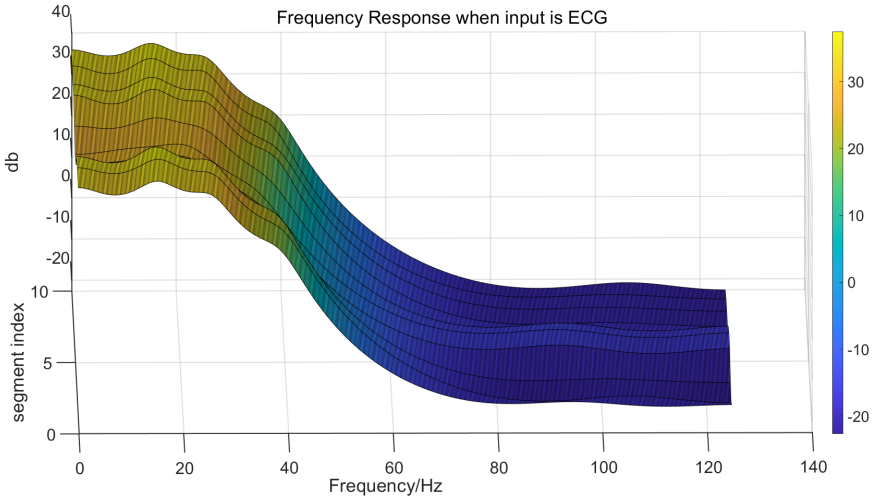

(a) Frequency response when input is the SR signal.

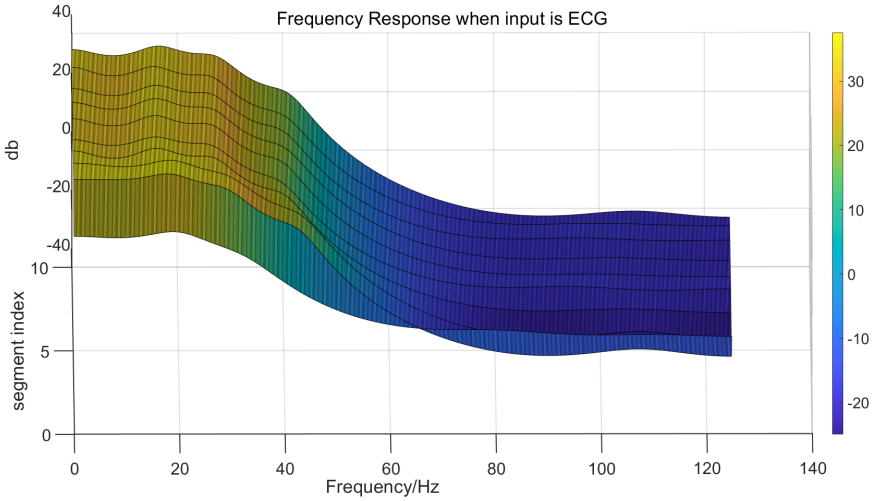

(b) Frequency response when input is the AF signal.

Figure 4.7: The frequency responses of AR models implemented on the SR ECG signal and the AF ECG signal.

Furthermore, the zero-pole plots in two cases are shown in Fig. 4.8. There are three clusters lying within the first quadrant in both cases, corresponding to three peaks in the responses. Other poles mainly contribute to modeling the noises. When AF happens, the distribution of poles becomes less concentrated, which is similar to the situation of only P-waves. However, the difference between the SR and AF cases is not as prominent as the situation of P-waves. By combining the responses and zero-pole plots of AR models, it can be concluded that ECG signals are not useful in this methodology. This is because P-waves are not prominent in the whole ECG signal. Even these weak waves are replaced by f-waves which have much less energy when AF happens. Under this circumstance, the parameters of the AR models can only reflect the contribution of QRST complexes, meaning that they mainly convey information about the ventricle, and it is hard to interpret the atrium information directly.

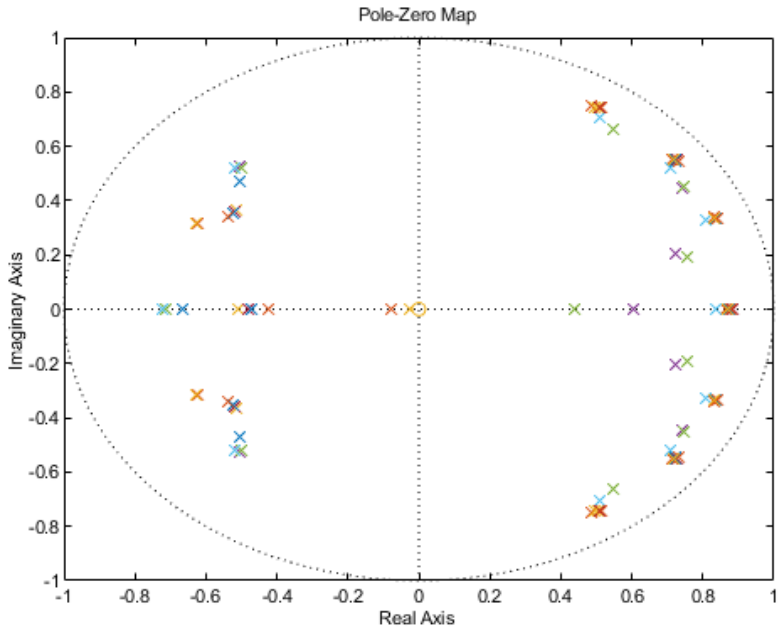

(a) Zero-pole plot when input is the SR signal.

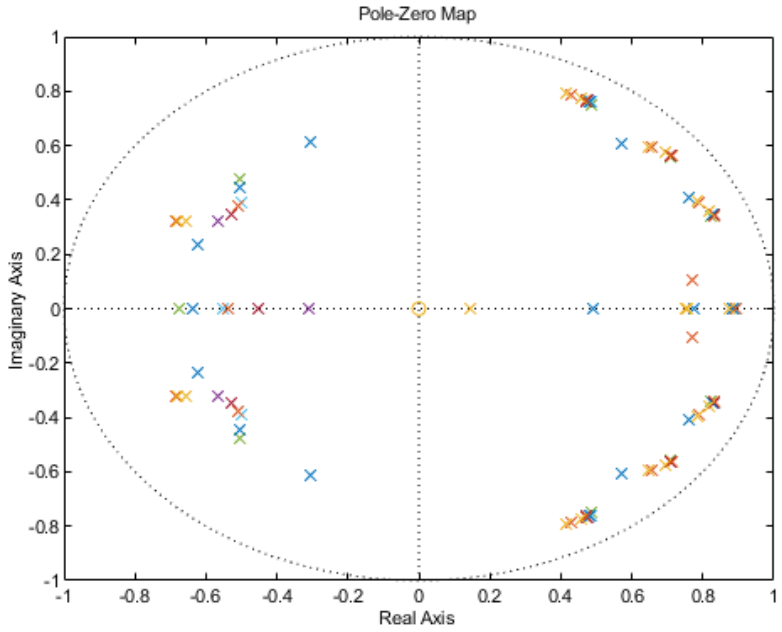

(b) Zero-pole plot when input is the AF signal.

Figure 4.8: The zero-pole plots of AR models implemented on the SR ECG signal and the AF ECG signal.

4.4 Chapter Summary

In this chapter, the interpretation of the information based on the model parameters is done. Firstly, the zero-pole plot is used to obtain information from the AR coefficients. This kind of plot can map these coefficients from 1-dimension to 2-dimensions such that they become sparse and high-dimension information can be acquired. In this case, the location of the first cluster of poles characterizes the formant which is a representation of how the atrium shapes input pulse trains. Besides, frequencies of formants are estimated. In the AF scenario, it can be observed the distribution of poles becomes dispersed and chaotic, implying that the atrium loses the capability of generating normal waves. In this case, the AF is interpreted at the signal level. Moreover, the signal level interpretation is linked with the physiological information of the atrium. Last, the complete ECG signal is implemented to explore whether the methodology is useful in the whole ECG recording. However, the results show that AF events can not be reflected in the intact recording. The possible reason is that P-waves and f-waves have weaker energy than QRST complexes and the model mainly focuses on QRST complexes.

Classification of SR and AF Signals

5

In this chapter, the classification process will be elaborated, which corresponds to the classification block in Fig. 1.1. To be specific, the criteria development will be shown first in Section. 5.1. Secondly, the identification of the parameters of the classifier will be discussed in Section. 5.2. Last, the classification results based on different metrics and the discussion will be illustrated in Section. 5.3.

5.1 Criteria Development

As described in the above section, the poles in the SR and the AF cases show different types of distributions, especially poles in the desired cluster which is marked by the red circle in Fig. 4.1. These desired poles in the SR case are more regular and more concentrated and located in a certain range. From the frequency perspective, the estimated formant frequencies $\hat{f}$ among different windows vary little, given the order of the AR model. In contrast, there is no regular and concentrated pattern for those desired poles in the AF situation. In this case, a classifier can be developed based on these obtained observations in order to classify SR recordings and AF recordings. It means the AF signal can be detected based on the AF mechanism derived from the model. Two criteria are used to build the classifier.

- The number of poles in the pre-defined region, which is a sector representing a frequency range from f_{lb} to f_{hb}, should not be less than m.
- The standard deviation of the desired clusters should be smaller than a threshold x.

The first criterion is made to identify the resonance frequency of P-waves. The pre-defined region actually implies the resonance frequency should lie within a certain range. A tolerance of $10 - m$ (The number of windows is 10) is given based on the observation that the estimated formant frequencies in the AF signal may be 0 Hz, and the consideration that the presence of noises and disturbances in P-waves will shift the frequencies represented by poles.

The second criterion is made to measure the degree of the concentration of poles. Since it is observed that the resonance frequencies across different windows do not change a lot, given the order of the AR model, it is possible to use the standard deviation to measure the distribution of the poles that represent the formant frequencies.

Hence, the signal will be classified as an SR signal if both criteria are met; otherwise an AF signal. The classifier and the decision-making process can be concluded as the table below.

	Number of poles in defined region $< m$	Number of poles in defined region $\geq m$
Standard deviation $< x$	AF	SR
Standard deviation $\geq x$	AF	AF

Table 5.1: Two criteria

Under this circumstance, the parameters which need to be determined are m, x, f_{lb}, f_{hb}, p. Recall p is the order of the AR model. The detailed parameters identification and results will be discussed in the next chapter.

5.2 Parameter Identification

As described above, there are several parameters required to be identified to define the classifier: the tolerance parameter m, the standard deviation threshold x, the lower bound and higher bound of the frequency region f_{lb}, f_{hb}, the order of the AR model p, and which window length method to be used. To find the optimized options of these parameters, the idea of alternating optimization is borrowed, which means some parameters are fixed whilst updating one parameter. This idea is exploited due to the fact that the program of classification will be too complex if all parameters are free and are updated simultaneously. In this case, some initial values should be considered to start the first update. These values are obtained based on observations of desired poles and estimated resonance frequencies by doing experiments on a small number of data (SR recording numbers: 16265, 16273, 16483, 16539, and AF recording numbers: 04908, 04936, 06995, 07879). The reason for choosing these recordings is just that they are the first several recordings of each dataset. The algorithm to determine parameters is listed in Algorithm. 3, and the detailed descriptions related to the setting of initial parameters are given in the following part.

Since the AR model with different orders is implemented in Chapter. 3 and 4, which is AR(8), AR(10), and AR(12), a deterministic order needs to be decided firstly. Besides, the choice of the type of window length should also be evaluated. The range of f_{lb} and f_{hb} are set by adding two units Hz on the initial value and subtracting two units Hz from the initial value. This range is enough to find the best frequency range, which will be shown in the following results. Besides, the minimum value of m is defined as five. The m specifies the minimum number of poles located outside the region, i.e., the tolerance. Ideally, for an SR recording, the poles representing the formants should always be located in the defined region, which means ten poles are all located in the region. However, this is not always the case due to the noises and artifacts. Therefore, the tolerance is introduced and denoted as m. If the number of poles in the defined region is larger than m, the recording can be considered as an SR recording. The minimum value of m is 5 because the total number of windows is 10 for each recording and 5 is half of the window number. If m is lower than 5, the tolerance is too loose since it permits more poles located outside the region than poles in the region, like 9 poles outside the region and only one pole in the region. In this case, the recording

Algorithm 3 Parameter Identification Algorithm

Input: $p \in \{8, 10, 12\}$, $x \in \{0, 0.0001, 0.0002, \ldots, 0.2\}$
Initialization: $m = 9, f_{lb} = 4, f_{hb} = 13$
for all p **do**
  for all x **do**
    Do classification on the dataset.
  end for
end for
Determine p_{best} and the best window length method based on metrics.
Input: $m \in \{5, 6, 7, 8, 9, 10\}$, p_{best}
Initialization: $f_{lb} = 4, f_{hb} = 13$
for all m **do**
  for all x **do**
    Do classification on the dataset.
  end for
end for
Determine m_{best} based on metrics.
Input: $f_{lb} \in \{2, 3, 4, 5, 6\}$, m_{best}, p_{best}
Initialization: $f_{hb} = 13$
for all f_{lb} **do**
  for all x **do**
    Do classification on the dataset.
  end for
end for
Input: $f_{hb} \in \{11, 12, 13, 14, 15\}$, m_{best}, p_{best}, f_{lb}^{best}
for all f_{hb} **do**
  for all x **do**
    Do classification on the dataset.
  end for
end for
Determine f_{hb}^{best} and x_{best} based on metrics.

can not be regarded as an SR recording and the tolerance does not function. Finally, the maximum value of the range of x is set to 0.2 because the maximum value of the standard deviation in the dataset is 0.1432. The step size of x is 0.0001 since the magnitude of the standard deviation of poles is very small.

In a word, these numbers and bounds are determined by enumerating all possible values alternatively. That is, some initial values of the parameters are first determined by the experiments of a batch of data. Then, the possible bounds of the parameters are proposed and enumerated based on the references or experiments to make the parameters more general and suitable for the dataset. For instance, since the frequency band of P-waves is below 15 Hz [22], the highest f_{hb} does not need to be set higher than 15 Hz. The range of the model's order has been proposed in Chapter. 3.5 based on the experiments.

It can be discovered that some bounds and values are dependent on the MIT-HIB SR

and AF datasets, i.e., data-dependent, like the m. This is reasonable since different patients across different datasets will exhibit different numerical values of these parameters. Besides, every classifier is driven by datasets. However, the logic of the algorithm and the idea are general and data-independent.

5.3 Results

In this thesis, the classification is implemented based on all recordings of the SR dataset and these recordings of the AF dataset which contain more than 200 beats AF signals, since the model requires 10 windows, each of which has 20 beats. The recordings used are summarized in the below table.

MIT-HIB SR dataset	MIT-HIB AF dataset
16265, 16272, 16273, 16483, 16539, 16773, 16786, 16795, 16420, 17052, 17453, 18177, 18184, 19088, 19090, 19093, 19140, 19830	04043, 04908, 04936, 06995, 07910, 08219, 08378, 08434, 08455

Table 5.2: Recordings used in this thesis.

The signals used for classification are obtained from these recordings. There are 72 signals obtained, with 36 SR signals and 36 AF signals. 54 signals among them are used to identify those parameters, and 18 signals are considered test set.

To evaluate those parameters, the receiver operating characteristic (ROC) curve and the area under the curve (AUC) are considered. The ROC curve is a graphical representation of the diagnostic ability of a binary classifier [62]. Particularly the AUC of a ROC curve quantifies the classification capability. The x-axis of the ROC is the false positive (FP) rate, and the y-axis of the ROC is the true positive (TP) rate. The FP rate and the TP rate are calculated by Eq. 5.1.

$$\begin{aligned} TP \quad rate &= \frac{TP}{P} = \frac{TP}{TP+FN} \\ FP \quad rate &= \frac{FP}{N} = \frac{FP}{FP+TN}, \end{aligned} \tag{5.1}$$

where FN represents the false negative, and TN means the true negative. In this thesis, the positive samples are AF signals. Hence,

Real label \ Classified label	AF	SR
AF	TP	FN
SR	FP	TN

Table 5.3: Confusion matrix. AF signals are positive samples, and SR signals are negative samples.

First, it is necessary the order of the AR model and the window length method used. As described in Chapter. 3.1.2 and Chapter. 3.5, AR models with different orders ranging from 8 to 12 are implemented on the signals extracted by MWL method and AWL method. The receiver operating characteristic (ROC) curve is used to evaluate the classification capability of the model with different orders and of different types of window length methods. Results are shown in Fig. 5.1. In addition, the AUC of these curves are listed in Table. 5.4, respectively. The AUC are computed by the area surrounded by the curve and the x-axis. It can be observed that in both types of window length, AR(10) has the highest AUC area that is computed by the area surrounded by the curve and the x-axis. In this case, $p = 10$ has the most powerful classification capability. Also, it can be discovered that when $p = 10$, the average window length method performs a higher AUC than the minimum window length method, which is about 0.907 for the former and approximately 0.893 for the latter. Thus, the average window length is preferred, and $p_{best} = 10$.

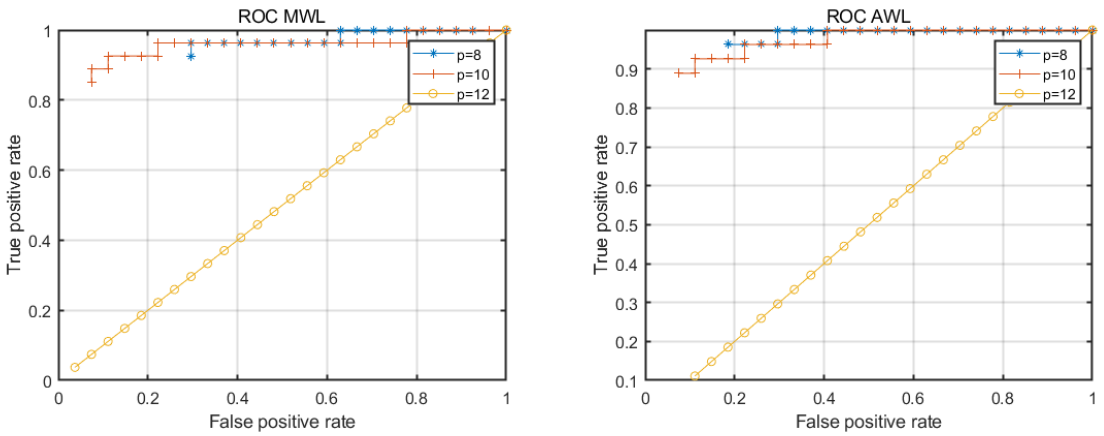

(a) ROC curve of the AR model with different orders in minimum window case.

(b) ROC curve of the AR model with different orders in average window case.

Figure 5.1: ROC for two window length method and different AR model orders.

Model Order	MWL	AWL
p=8	0.731	0.811
p=10	0.893	0.907
p=12	0.500	0.450

Table 5.4: AUC of AR models with different orders and two window methods.

After the appropriate order $p = 10$ and the average window length method are determined, there are still four parameters required to be identified. To determine m, the ROC curve is still used, which is plotted in (a) in Fig. 5.2. Besides, the accuracy is shown in (b) in the figure. What has to be mentioned is that the accuracy curves of $m = 8$ and $m = 9$ coincide after about threshold $x = 0.06$. In this case, the $m = 8$ and $m = 9$ perform comparative results, i.e., similar ROC curves and the same accu-

racy. Hence, the AUC of these curves are listed in Table. 5.5 to better determine the parameter. The table shows that $m = 7$ has the highest AUC of 0.937, whereas $m = 8$ has the second highest one of 0.933. Although the AUC of $m = 7$ is 0.004 higher than the AUC of $m = 8$, their values are similar, and the accuracy of $m = 8$ is much higher than that of $m = 7$, where the former is more than 90% and the latter is around 85%. Hence, $m = 8$ is a better option than $m = 7$. As for $m = 9$ and $m = 8$, the AUC of $m = 9$ is 0.907, which is a bit lower than that of $m = 8$. As a result, $m = 8$ is the best option by combining the ROC curve and the accuracy.

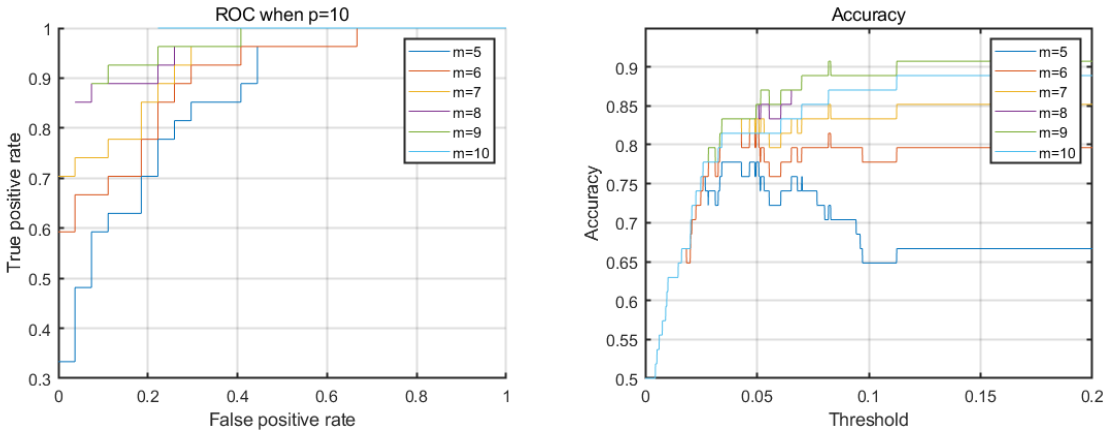

(a) ROC curve of the AR model whilst determining m_{best}

(b) Accuracy curve of the AR model whilst determining m_{best}

Figure 5.2: ROC and accuracy curves of the model whilst determining m_{best}, given $p = 8$ and using the AWL method.

m	AUC
m=5	0.894
m=6	0.902
m=7	0.937
m=8	0.933
m=9	0.907
m=10	0.778

Table 5.5: AUC value whilst determining m_{best}, given $p = 12$ and using the AWL method.

Next, it moves to determine f_{lb}^{best}. In this case, only the accuracy is used to reveal which f_{lb} is the best. The algorithm traverses the range of f_{lb} mentioned before. The results are shown in Fig. 5.3. It shows when f_{lb} increases from 2 Hz to 5 Hz, the accuracy curve increases. In this case, the values of f_{lb} lower than 2 Hz do not need to be considered. But if the lower bound increases from 5 Hz to 6 Hz, the accuracy declines. Hence, $f_{lb} = 5$ Hz has the highest accuracy. In addition. the accuracy of $f_{lb} = 6$ Hz is lower than that of $f_{lb} = 5$ Hz, which proves the range of f_{lb} is appropriate enough because if the lower bound continues increasing, more and more frequency artifacts will

be included. As a result, it can be concluded that $f_{lb}^{best} = 5$ Hz. Moreover, this value is in line with the expectation that in most cases the formant frequency is more than 5 Hz, like the peak of 7 Hz in Fig. 2.5. However, no exact value of this has been proposed in the literature. Usually, P-waves are considered more than 0 Hz. The concept of the frequency band is frequently used, instead of the formant.

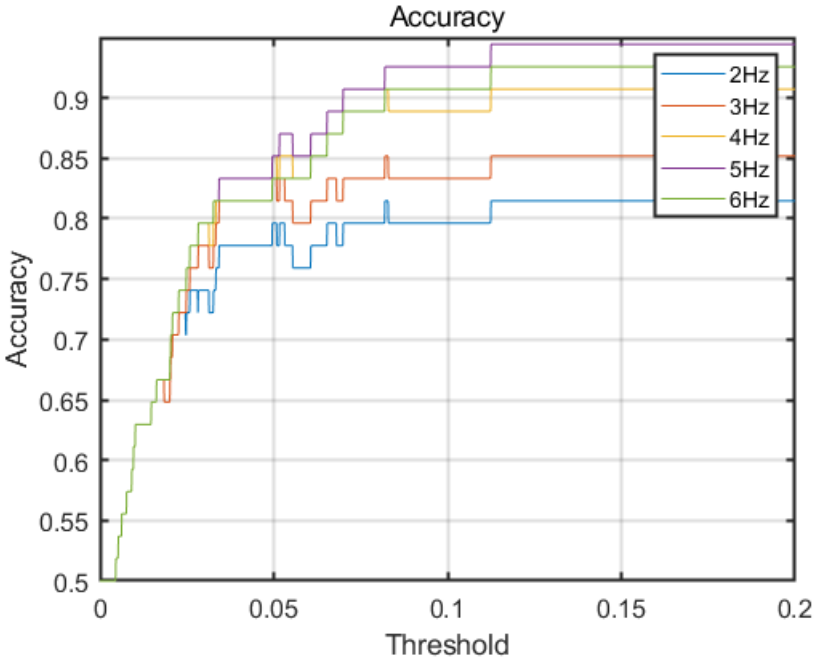

Figure 5.3: Accuracy of the AR model with different options of f_{lb}

Finally, the higher bound of the frequency range, f_{hb}^{best}, should be identified. Similarly, the accuracy curves are utilized to determine f_{hb}^{best} by fixing $f_{lb}^{best} = 5$ Hz, shown in Fig. 5.4. This figure reveals that these curves do not perform a wide difference, which differs from the lower bound case. These curves differ at some thresholds but coincide at last. To be specific, $f_{hb} = 11$ Hz can be considered to have the lowest accuracy. The $f_{hb} = 15$ Hz is slightly better than $f_{hb} = 11$ Hz since it becomes higher when x lies within the range from about 0.0696 to 0.0927 regardless of the final coincidence. In a similar manner, the $f_{hb} = 12$ Hz has a bit worse performance than $f_{hb} = 14$ Hz since the latter possesses a higher accuracy when x lies within the range from about 0.0696 to 0.0927. $f_{hb} = 13$ Hz has the same accuracy as the case of 14 Hz before 0.0927 and then becomes the highest one. In this case, f_{hb}^{best} is 13 Hz. This value is actually unexpectedly high because it lies within the possible values of the higher bound of P-waves' frequency bound which is 10 to 15 Hz [22], whereas the frequency of the formant representing the most signal energy is ideally lower than the bound.

In addition, the accuracy reaches its highest value and does not change after the threshold x reaches a particular value. This phenomenon actually implies that all signals satisfy the second criterion. In other words, for every data, the desired cluster of poles has a standard deviation smaller than x, which can be understood by eliminating the

third row of Table.5.1. In this case, the only functioning criterion is the first one, and the accuracy of almost 95% is really high. Hence, one option of x is to consider the first value, $x^{best} = 0.1125$, where the accuracy becomes the highest of all values. In this case, choices of all parameters can be summarized in Table. 5.6

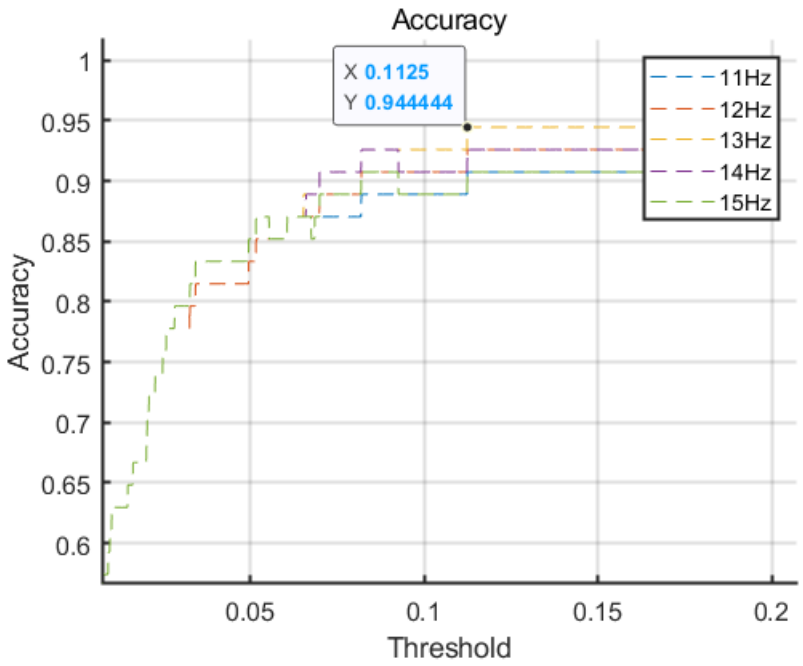

Figure 5.4: Accuracy of the AR model with different options of f_{hb}

Parameter	Choice
Window method	AWL
Model order	10
tolerance parameter m	8
f_{lb}	5 Hz
f_{hb}	13 Hz
threshold x	0.1125

Table 5.6: The final parameters determined.

After all parameters are determined, the classifier is implemented on the test set in order to become a general model. The accuracy curve over all thresholds is shown in Fig. 5.5. It can be observed that the curve does not exactly match the curve of determining parameters. For instance, the curve of determining parameters performs an overall increasing trend, whereas the curve of the test set has a peak at around 0.045. At this moment, there are 8 true negative samples and 9 true positive samples, which means an SR signal is classified as the AF class. By observing the data, it can be found that one SR signal has a high standard deviation of 0.0544 due to large noises and thus is classified incorrectly. If the threshold x is set to 0.1125, the accuracy will be

88.9% in the test set, which is still a high value. In this case, there are 7 true positive samples and 9 true negative ones, implying that two AF signals are undetected. It is because their estimated frequencies meet the tolerance of 8. Meanwhile, the threshold is a little big though their standard deviation is big even if they can be found as AF signals from the zero-pole plots.

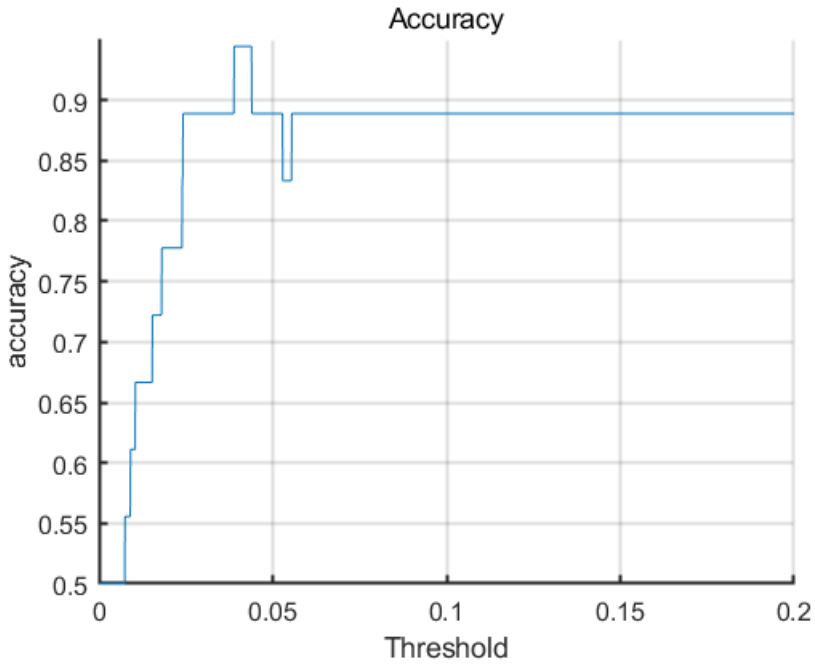

Figure 5.5: Accuracy of the model implemented on the test set.

5.4 Chapter Summary

In this chapter, a parametric classifier based on the information obtained in the last chapter is proposed. Since the classifier is parametric and the information is explicit, the classifier can be considered interpretable. In addition, an alternating algorithm is proposed to determine parameters in the classifier. The possible values of the parameters are enumerated to identify the best parameters. The ROC, AUC, and accuracy are used as metrics to evaluate the performance. The final set of the parameters is shown in Table. 5.6.

6 Conclusion and Future Work

ECG is a type of non-invasive measurement of the heart and is widely-used in the clinical scenario due to its easily-implemented characteristic. P-waves are the components reflecting atrial activities in the ECG signal, meaning that modeling P-waves allows to interpret information related to the atrium. AF is a common cardiac illness which can trigger deadly complications. Although tens of millions of people are suffering from it, its underlying mechanisms are not completely understood. In this case, modeling P-waves provide a way to interpret AF mechanisms at the signal-processing level.

In Chapter 3, this thesis has modeled P-waves of SR and AF signals by the AR model, which is also called LPC in the acoustic signal processing domain, and the ARMA model that can theoretically achieve the same modeling performance with lower orders. To achieve this, the raw ECG signal was filtered and delineated by pre-processing steps. The choice of the order was initially considered in terms of the AIC value and finally identified by the correlation removal. Besides, the AR model and ARMA model were compared based on the evaluation of the correlation removal in order to decide which model was more preferred. The function of the atrium imposed on the impulse trains, which is the output of the SA node, was represented by this de-correlation model in this manner. In other words, the proposed model played a role of the atrium from the signal perspective. Although the explicit order is not decided, the AR model with the Burg method was determined as the most appropriate model in this chapter.

Chapter 4 was subsequently concerned with the interpretation of results of the model. Parameters of the model were characterized by poles in zero-pole plots of the filter. In addition, the information of the atrium was modeled as the formant which was a type of representation of speech signals. Resonance frequencies of formants were also estimated. The relationship between the signal level interpretation and the physiology nature of the heart is built. Moreover, the intact ECG signal is modeled by the proposed model, and the results are compared with the P-waves case. The results showed AF components could not be revealed in the ECG modeling case. It was possibly due to the fact that AF activities have lower energy than the normal P-waves and were hidden by the large energy of QRST complexes. In a word, this chapter described how the atrium activated at the signal level, namely generating P-waves and f-waves.

Afterward, in Chapter 5, an interpretable parametric classifier was derived in terms of differences in LPC coefficients and formants between SR signals and AF signals. An alternative decision-making algorithm was proposed to determine the parameters of the classifier based on the training set. The metrics used are ROC curves, AUC, and accuracy. With these parameters determined and summarized in Table. 5.6, the classifier achieves high accuracy based on the dataset, 94.4% in the training set, and 88.9% in the test set.

This thesis provides a novel understanding of the atrium functioning P-waves and the pathogenic principle of AF at the signal level. Based on the parameters of the proposed model, it gives the formant interpretation of the atrium and describes the generation of P-waves and f-waves, which is beneficial for understanding the underlying AF mechanisms and early detection. The interpretation made is also connected with the physiology of the atrium. In this way, the signal level information reflects the physiological information. Besides, The overall model only requires the single-lead ECG and thus is easy to implement on the patients. In this case, the parametric classifier can be deployed easily, unlike the multi-lead ECG recordings which may require patients to wear several hours. Due to the single-lead feature of the overall model, the work of this thesis provides potential benefits to self-check of patients, like using wearable devices in the future.

6.1 Future Work

One future work is to address limitations, mainly of which are brought by the pre-processing step. The first limitation is its robustness to the noises. Although the baseline wander at 0.6 Hz and the powerline interference at 50 Hz were removed in the pre-processing step, noises caused by muscle activities and the electrode motion artifacts were not tackled specially. Their existence will influence the modeling of the model and the concentration of poles and thus doing harm to the classification performance. Secondly, in order to reduce the noise at around 1.2 Hz, the cut-off frequency of the highpass filter is extended from 0.6 to 1.3 Hz, leading that some energy of P-waves was also removed. The source of this kind of noise was not explored in detail. If it is understood completely, a better solution can be derived to filter this kind of noise and preserve P-waves. Thirdly, the P-waves were delineated by subtracting QRST complexes from the intact ECG signal. The window of QRST complexes used is a rectangular window and thus caused discontinuity of post-processing P-waves. Besides, the window length is manually decided based on the minimum RR interval or the average RR interval. Therefore, it is not adaptive and may not be suitable for all QRST complexes, meaning not all desired atrial components are preserved, and not all QRST complexes are removed. These limitations can be the direction of future work.

In addition, another future work can be collecting more data. The present dataset is not at a big scale that may not be representative enough for the final parameters identification. Enlarging the dataset will improve this perspective. Moreover, future work can consider more ways to interpret formants and resonance frequencies, like line spectral frequency, mel-frequency cepstral coefficients, and linear-frequency cepstral coefficients. Lastly, another methodology can be considered to model the atrium, instead of the formant. The idea is to use an adaptive filter to minimize the MSE,

$$min||s - \mathbf{w}^H\mathbf{x}||^2, \tag{6.1}$$

where s represents the pulse train, and $\mathbf{x}$ denotes the P-waves. The w specifies the filter weights. Since the pulse train is hard to obtain, the simulated pulse train generated by the IPFM model can be considered as an alternative option. The parameters of the

IPFM model can be determined based on real ECG recordings. The schematic diagram of the idea is plotted in Fig. 6.1.

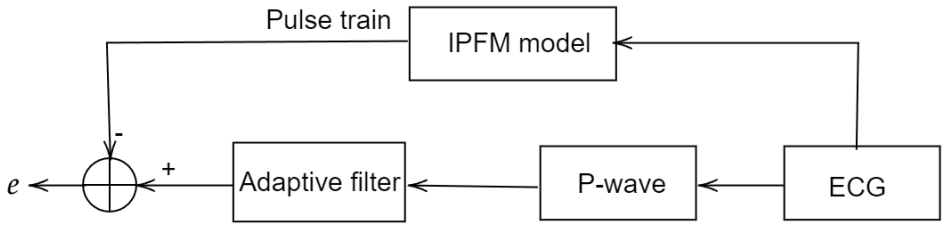

Figure 6.1: The schematic diagram of the new idea. The e represents the MSE of the pulse train and the output of the adaptive filter.

Bibliography

[1] NHS. *Atrial fibrillation*. May 2021. URL: https://www.nhs.uk/conditions/atrial-fibrillation/.

[2] Larissa Fabritz et al. "Expert consensus document: defining the major health modifiers causing atrial fibrillation: a roadmap to underpin personalized prevention and treatment". In: *Nature reviews. Cardiology* 13.4 (2016), p. 230.

[3] Massimo Zoni-Berisso et al. "Epidemiology of atrial fibrillation: European perspective". In: *Clinical epidemiology* (2014), pp. 213–220.

[4] Larissa Fabritz et al. "Personalized management of atrial fibrillation". In: *ESC CardioMed (3 ed.)* Oxford University Press, 2018.

[5] Gabriel E. Arrobo et al. "An innovative wireless Cardiac Rhythm Management (iCRM) system". In: *2014 Wireless Telecommunications Symposium*. 2014, pp. 1–5. DOI: 10.1109/WTS.2014.6835035.

[6] Dominique Méry and Neeraj Kumar Singh. "Technical report on formal development of two-electrode cardiac pacing system". In: (2010).

[7] Wikipedia. *Sinoatrial node*. Apr. 2023. URL: https://en.wikipedia.org/wiki/Sinoatrial_node.

[8] AK Lectures. *Action Potential vs. Muscle Contraction Graphs*. Sept. 2014. URL: https://aklectures.com/lecture/muscular-system/action-potential-vs-muscle-contraction-graphs.

[9] LibreTexts. *The Action Potential and Propagation*. [Online; accessed 2023-06-05]. Jan. 2023.

[10] Andrei D Margulescu and Lluis Mont. "Persistent atrial fibrillation vs paroxysmal atrial fibrillation: differences in management". In: *Expert review of cardiovascular therapy* 15.8 (2017), pp. 601–618.

[11] EN Simantirakis et al. "Asymptomatic versus symptomatic episodes in patients with paroxysmal atrial fibrillation via long-term monitoring with implantable loop recorders". In: *International Journal of Cardiology* 231 (2017), pp. 125–130.

[12] Michel Haissaguerre et al. "Right and left atrial radiofrequency catheter therapy of paroxysmal atrial fibrillation". In: *Journal of cardiovascular electrophysiology* 7.12 (1996), pp. 1132–1144.

[13] Mélèze Hocini et al. "Electrical conduction in canine pulmonary veins: electrophysiological and anatomic correlation". In: *Circulation* 105.20 (2002), pp. 2442–2448.

[14] Laila Staerk et al. "Atrial fibrillation: epidemiology, pathophysiology, and clinical outcomes". In: *Circulation research* 120.9 (2017), pp. 1501–1517.

[15] HANS KOTTKAMP. "Fibrotic Atrial Cardiomyopathy: A Specific Disease/Syndrome Supplying Substrates for Atrial Fibrillation, Atrial Tachycardia, Sinus Node Disease, AV Node Disease, and Thromboembolic Complications". In: *Journal of Cardiovascular Electrophysiology* 23.7 (2012), pp. 797–799. DOI: https://doi.org/10.1111/j.1540-8167.2012.02341.x. eprint: https://onlinelibrary.wiley.com/doi/pdf/10.1111/j.1540-8167.2012.02341.x.

URL: https://onlinelibrary.wiley.com/doi/abs/10.1111/j.1540-8167.2012.02341.x.

[16] Paulus Kirchhof et al. "2016 ESC Guidelines for the management of atrial fibrillation developed in collaboration with EACTS". In: *European Heart Journal* 37.38 (Aug. 2016), pp. 2893–2962. ISSN: 0195-668X. DOI: 10.1093/eurheartj/ehw210. eprint: https://academic.oup.com/eurheartj/article-pdf/37/38/2893/23787249/ehw210.pdf. URL: https://doi.org/10.1093/eurheartj/ehw210.

[17] Leif Sörnmo, A Petrėnas, and V Marozas. *Atrial fibrillation from an engineering perspective*. Springer, 2018.

[18] Wikipedia. *Electrocardiography*. Sept. 2022. URL: https://en.wikipedia.org/wiki/Electrocardiography.

[19] Ziad F. Issa, John M. Miller, and Douglas P. Zipes. "Chapter 8 - Sinus Node Dysfunction". In: *Clinical Arrhythmology and Electrophysiology: A Companion to Braunwald's Heart Disease (Second Edition)*. Ed. by Ziad F. Issa, John M. Miller, and Douglas P. Zipes. Second Edition. Philadelphia: W.B. Saunders, 2012, pp. 164–174. ISBN: 978-1-4557-1274-8. DOI: https://doi.org/10.1016/B978-1-4557-1274-8.00008-7. URL: https://www.sciencedirect.com/science/article/pii/B9781455712748000087.

[20] Fumihiko Yasuma and Jun-ichiro Hayano. "Respiratory Sinus Arrhythmia: Why Does the Heartbeat Synchronize With Respiratory Rhythm?" In: *Chest* 125.2 (2004), pp. 683–690. ISSN: 0012-3692. DOI: https://doi.org/10.1378/chest.125.2.683. URL: https://www.sciencedirect.com/science/article/pii/S001236921531878X.

[21] Francisco Azuaje, Gari Clifford, and Patrick McSharry. 2006.

[22] Leif Sörnmo and Pablo Laguna. *Bioelectrical signal processing in cardiac and neurological applications*. Vol. 8. Academic press, 2005.

[23] Wikipedia. *Autoregressive model*. May 2023. URL: https://en.wikipedia.org/wiki/Autoregressive_model#cite_note-1.

[24] Dalibor Mitrović, Matthias Zeppelzauer, and Christian Breiteneder. "Chapter 3 - Features for Content-Based Audio Retrieval". In: *Advances in Computers: Improving the Web*. Vol. 78. Advances in Computers. Elsevier, 2010, pp. 71–150. DOI: https://doi.org/10.1016/S0065-2458(10)78003-7. URL: https://www.sciencedirect.com/science/article/pii/S0065245810780037.

[25] Gang Wang et al. "Extraction of desired signal based on AR model with its application to atrial activity estimation in atrial fibrillation". In: *EURASIP Journal on Advances in Signal Processing* 2008 (2008), pp. 1–9.

[26] D. O'Shaughnessy. "Linear predictive coding". In: *IEEE Potentials* 7.1 (1988), pp. 29–32. DOI: 10.1109/45.1890.

[27] B. S. Atal and M. R. Schroeder. "Adaptive predictive coding of speech signals". In: *The Bell System Technical Journal* 49.8 (1970), pp. 1973–1986. DOI: 10.1002/j.1538-7305.1970.tb04297.x.

[28] J. Makhoul. "Linear prediction: A tutorial review". In: *Proceedings of the IEEE* 63.4 (1975), pp. 561–580. DOI: 10.1109/PROC.1975.9792.

[29] Wikipedia. *Linear predictive coding*. Apr. 2023. URL: https://en.wikipedia.org/wiki/Linear_predictive_coding.

[30] Wikipedia. *Autoregressive–moving-average model*. Apr. 2023. URL: https://en.wikipedia.org/wiki/Autoregressive%5C%E2%5C%80%5C%93moving-average_model.

[31] P Bonizzi et al. "Ventricular activity residual reduction in remainder ECGs based on short-term autoregressive model interpolation". In: *2009 36th Annual Computers in Cardiology Conference (CinC)*. 2009, pp. 813–816.

[32] Dingfei Ge, Narayanan Srinivasan, and Shankar M Krishnan. "Cardiac arrhythmia classification using autoregressive modeling". In: *Biomedical engineering online* 1.1 (2002), pp. 1–12.

[33] K. Padmavathi and K. Sri Ramakrishna. "Classification of ECG Signal during Atrial Fibrillation Using Autoregressive Modeling". In: *Procedia Computer Science* 46 (2015). Proceedings of the International Conference on Information and Communication Technologies, ICICT 2014, 3-5 December 2014 at Bolgatty Palace Island Resort, Kochi, India, pp. 53–59. ISSN: 1877-0509. DOI: https://doi.org/10.1016/j.procs.2015.01.053. URL: https://www.sciencedirect.com/science/article/pii/S187705091500054X.

[34] Varun Gupta and Monika Mittal. "KNN and PCA classifier with Autoregressive modelling during different ECG signal interpretation". In: *Procedia Computer Science* 125 (2018). The 6th International Conference on Smart Computing and Communications, pp. 18–24. ISSN: 1877-0509. DOI: https://doi.org/10.1016/j.procs.2017.12.005. URL: https://www.sciencedirect.com/science/article/pii/S1877050917327692.

[35] Rahul Kher et al. "Signal processing techniques for removing noise from ECG signals". In: *J. Biomed. Eng. Res* 3.101 (2019), pp. 1–9.

[36] Noura AlHinai. "Chapter 1 - Introduction to biomedical signal processing and artificial intelligence". In: *Biomedical Signal Processing and Artificial Intelligence in Healthcare*. Ed. by Walid Zgallai. Developments in Biomedical Engineering and Bioelectronics. Academic Press, 2020, pp. 1–28. DOI: https://doi.org/10.1016/B978-0-12-818946-7.00001-9. URL: https://www.sciencedirect.com/science/article/pii/B9780128189467000019.

[37] Saeed Mian Qaisar. "Baseline wander and power-line interference elimination of ECG signals using efficient signal-piloted filtering". In: *Healthcare Technology Letters* 7.4 (2020), pp. 114–118. DOI: https://doi.org/10.1049/htl.2019.0116. eprint: https://ietresearch.onlinelibrary.wiley.com/doi/pdf/10.1049/htl.2019.0116. URL: https://ietresearch.onlinelibrary.wiley.com/doi/abs/10.1049/htl.2019.0116.

[38] Ary L Goldberger et al. "PhysioBank, PhysioToolkit, and PhysioNet: components of a new research resource for complex physiologic signals". In: *circulation* 101.23 (2000), e215–e220.

[39] Jonathan Moeyersons et al. "R-DECO: An open-source Matlab based graphical user interface for the detection and correction of R-peaks". In: *Peerj computer science* 5 (2019), e226.

[40] Carolina Varon et al. "A Novel Algorithm for the Automatic Detection of Sleep Apnea From Single-Lead ECG". In: *IEEE Transactions on Biomedical Engineering* 62.9 (2015), pp. 2269–2278. DOI: 10.1109/TBME.2015.2422378.

[41] Wikipedia. *Pan–Tompkins algorithm*. Jan. 2023. URL: https://en.wikipedia.org/wiki/Pan%5C%E2%5C%80%5C%93Tompkins_algorithm.

[42] Philip De Chazal et al. "Automated processing of the single-lead electrocardiogram for the detection of obstructive sleep apnoea". In: *IEEE transactions on biomedical engineering* 50.6 (2003), pp. 686–696.

[43] Anupreet Kaur Singh and Sridhar Krishnan. "ECG signal feature extraction trends in methods and applications". In: *BioMedical Engineering OnLine* 22.1 (2023), pp. 1–36.

[44] Sridhar Krishnan and Yashodhan Athavale. "Trends in biomedical signal feature extraction". In: *Biomedical Signal Processing and Control* 43 (2018), pp. 41–63. ISSN: 1746-8094. DOI: https://doi.org/10.1016/j.bspc.2018.02.008. URL: https://www.sciencedirect.com/science/article/pii/S1746809418300399.

[45] Russell Davidson, James G MacKinnon, et al. *Econometric theory and methods*. Vol. 5. Oxford University Press New York, 2004.

[46] P.K. Bhattacharya and Prabir Burman. "13 - Time Series". In: *Theory and Methods of Statistics*. Ed. by P.K. Bhattacharya and Prabir Burman. Academic Press, 2016, pp. 431–489. ISBN: 978-0-12-802440-9. DOI: https://doi.org/10.1016/B978-0-12-802440-9.00013-8. URL: https://www.sciencedirect.com/science/article/pii/B9780128024409000138.

[47] Wikipedia. *Pearson correlation coefficient*. June 2023. URL: https://en.wikipedia.org/wiki/Pearson_correlation_coefficient.

[48] Petre Stoica, Randolph L Moses, et al. *Spectral analysis of signals*. Vol. 452. Pearson Prentice Hall Upper Saddle River, NJ, 2005.

[49] L. Ljung. *System Identification: Theory for the User*. Prentice Hall information and system sciences series. Prentice Hall PTR, 1999. ISBN: 9780136566953. URL: https://books.google.nl/books?id=nHFoQgAACAAJ.

[50] R. Bos, S. de Waele, and P.M.T. Broersen. "Autoregressive spectral estimation by application of the Burg algorithm to irregularly sampled data". In: *IEEE Transactions on Instrumentation and Measurement* 51.6 (2002), pp. 1289–1294. DOI: 10.1109/TIM.2002.808031.

[51] James Douglas Hamilton. *Time series analysis*. Princeton university press, 2020.

[52] G.E.P. Box and G.M. Jenkins. *Time Series Analysis: Forecasting and Control*. Holden-Day series in time series analysis and digital processing. Holden-Day, 1976. ISBN: 9780816211043. URL: https://books.google.nl/books?id=1WVHAAAAMAAJ.

[53] Henrik Madsen. *Time series analysis*. English. Chapman Hall, 2007. ISBN: 9780429195839. DOI: 10.1201/9781420059687.

[54] Lisa Sullivan. *Confidence Intervals*. Oct. 2017. URL: https://sphweb.bumc.bu.edu/otlt/mph-modules/bs/bs704_confidence_intervals/bs704_confidence_intervals_print.html.

[55] G.E.P. Box et al. *Time Series Analysis: Forecasting and Control*. Wiley Series in Probability and Statistics. Wiley, 2015. ISBN: 9781118674925. URL: https://books.google.nl/books?id=rNt5CgAAQBAJ.

[56] Wikipedia. *Akaike information criterion*. June 2023. URL: https://en.wikipedia.org/wiki/Akaike_information_criterion.

[57] Wikipedia. *Bayesian information criterion*. Apr. 2023. URL: https://en.wikipedia.org/wiki/Bayesian_information_criterion.

[58] P.E. McSharry et al. "A dynamical model for generating synthetic electrocardiogram signals". In: *IEEE Transactions on Biomedical Engineering* 50.3 (2003), pp. 289–294. DOI: 10.1109/TBME.2003.808805.

[59] Wikipedia. *Runge–Kutta methods*. Apr. 2023. URL: https://en.wikipedia.org/wiki/Runge%5C%E2%5C%80%5C%93Kutta_methods.

[60] Roger G. Mark George B. Moody. "A new method for detecting atrial fibrillation using R-R intervals". In: *Computers in Cardiology* 10 (1983), pp. 227–230.

[61] Cheng Guo, Sajid Ahmed, and Mohamed-Slim Alouini. *Machine Learning-Based Automatic Cardiovascular Disease Diagnosis Using Two ECG Leads*. 2023. arXiv: 2305.16055 [eess.SP].

[62] Wikipedia. *Receiver operating characteristic*. July 2023. URL: https://en.wikipedia.org/wiki/Receiver_operating_characteristic.